ASTRONOMY & ASTROPHYSICS
SUPPLEMENT SERIES

Astron. Astrophys. Suppl. Ser. **126,** 437-469 (1997)

Spatial and kinematic properties of the forbidden emission line region of T Tauri stars

G.A. Hirth[1], **R. Mundt**[1], **and J. Solf**[2]

[1] Max-Planck-Institut für Astronomie, Königstuhl 17, D-69117 Heidelberg, Germany
[2] Thüringer Landessternwarte Tautenburg, Sternwarte 5, D-07778 Tautenburg, Germany

Received December 2, 1996; accepted April 15, 1997

Abstract. We have carried out a long-slit spectroscopic survey for 38 T Tauri stars (TTSs) to study the spatial and kinematic properties of their forbidden emission line (FEL) regions. With these observations we hope to provide more insight into the complex physical structure of the outflows from young stars on the smallest spatial scales observable by long-slit spectroscopy. Due to the differential nature of the observational method, information on the spatial properties (offset from the stellar continuum and spatial width) on sub-arcsec (sub-seeing) scales can be obtained. For most TTSs the [OI] $\lambda\lambda$6300, 6363, [NII] λ6583 and [SII] $\lambda\lambda$6716, 6731 lines have been investigated at a typical spatial resolution of 1.5″ and a velocity resolution of $20 - 50$ km s^{-1}. A sub-sample of 9 closeby stars (Haro 6-10, XZ Tau, UZ Tau E, HN Tau, DO Tau, DP Tau, UY Aur, RW Aur and V536 Aql) has been extensively studied and the direction of their outflows has been approximately determined by taking spectra at several slit position angles, if not known from emission-line CCD imaging. The spatial and kinematic properties of the FEL regions of these 9 TTSs are described in detail. Together with 3 additional stars discussed in the literature, a sample of 12 stars provides the basis for the following main results of our survey: The so-called high-velocity component (HVC) of the FELs (or gas of high velocity which presumably represents in many cases a HVC being blended with emission of lower velocity) is generally spatially more extended than the so-called low-velocity component (LVC, or gas near the stellar velocity). In the [SII] λ6731 line the centroid of the high-velocity gas is located typically at distances of 0.6″ from the TTS while for the low-velocity gas this value is smaller on average by more than a factor of 3. Comparing the spatial properties of the high-velocity gas among the investigated FELs, it turns out that the largest spatial width and the largest offset of the centroid from the star is usually observed in the [NII] λ6583 line, while the emission region is most compact in the [OI] λ6300 line. In [OI] the centroid of the high-velocity gas is typically offset by only 0.2″ from the star whereas in [SII] and [NII] 3 and 3.5 times larger average values have been measured, respectively. In the case of the low-velocity gas, the smallest offset of the emission centroid is also observed in [OI] (typically 0.1″ in [OI] and 0.2″ in [SII]).

Our data provide additional support for the model of Kwan & Tademaru (1988, 1995) according to which the HVC observed in the FELs of many TTSs is formed in a well-collimated jet, while the LVC represents gas from a physically distinct flow component (possibly a disk wind or a disk corona). The larger spatial extent of the high-velocity gas in [SII] and [NII] compared to that in [OI] is most probably the result of a jet decreasing in density with increasing distance from the source combined with an increase in excitation. The decrease of the electron density with distance is rather obvious for a jet with diverging stream lines, but why the electron temperature increases is unclear.

Key words: stars: pre-main-sequence — stars: variable — stars: emission-line — ISM: jets and outflows

1. Introduction

Spectroscopic studies of the forbidden emission lines (FELs) of T Tauri stars (TTSs), like the [OI] $\lambda\lambda$6300, 6363 and the [SII] $\lambda\lambda$6716, 6731 lines, have shown that these lines serve as powerful probes of the outflow activity of young stellar objects (YSOs) (see e.g. Appenzeller & Mundt 1989 or Edwards et al. 1993 for a review). Particularly for more evolved YSOs which are no longer deeply embedded in their parental molecular cloud and are therefore probably more evolved, the FELs often serve as the only diagnostic mean to investigate their outflows, since these YSOs are usually not associated with Herbig-Haro (HH) objects or HH jets.

Send offprint requests to: R. Mundt

FELs occur relatively frequently in YSOs, e.g. about 30% of all TTSs show strong FELs with $W_\lambda > 1$ Å for the [OI] λ6300 line (Cohen & Kuhi 1979), while the [SII] $\lambda\lambda$6716, 6731 lines are far less often detected probably because of their typically 5 times smaller flux.

Line profile data of the FELs for about 45 TTSs are presently available in the literature (e.g. Appenzeller et al. 1984; Edwards et al. 1987; Hamann 1994; Hartigan et al. 1995). In many cases the FELs are blueshifted and furthermore often double-peaked profiles are observed. The so-called high-velocity component (HVC) of this double-peaked profile has typical radial velocities between -50 and -150 km s^{-1} while the so called low-velocity component (LVC) has values around -5 to -20 km s^{-1}. Already Jankovics et al. (1983) concluded from the similar velocity distributions of HH objects and the blueshift of the FELs that these lines form in anisotropic bipolar outflows. According to this scenario, which is still basic to all models of FEL formation, an optically thick circumstellar disk, obscures the majority of the receeding part of the bipolar outflow. Therefore in most cases only blueshifted FELs are observed. However, it should be noted that in the higher S/N ratio data nowadays available more and more cases have been found where both sides of the bipolar outflow have been detected.

The nature of the HVC and LVC has been heavily discussed in the literature. In most cases it has been tried to interpret the two components by a single flow component viewed under favourable inclination angles (e.g. Edwards et al. 1987; Hartmann & Raymond 1989; Gómez de Castro & Pudritz 1993; Ouyed & Pudritz 1993, 1994). However, from the available line profile data and particular from various long-slit spectroscopic studies (e.g. Solf 1989; Solf & Böhm 1993; Böhm & Solf 1994; Hirth et al. 1994a; Hirth et al. 1994b) a different picture emerged. It is most likely from these data that the HVC and LVC represent two *physically distinct* flow components, with the LVC being spatially much more compact, of lower excitation and usually of higher density. Furthermore the long-slit data provide now very strong arguments that the HVC forms in a jet (Hirth et al. 1994a), as first proposed by Kwan & Tademaru (1988), while the nature of the LVC is still a matter of debate. Kwan & Tademaru (1988, 1995) suggested that the LVC is formed in a disk wind or disk corona. It is also conceivable that this component originates in the boundary layer in the innermost part of the jet. This might also explain, why the LVC becomes faster and more tenuous with increasing distance from the source as observed in DG Tau (Solf & Böhm 1993) and CW Tau (Hirth et al. 1994a).

In order to understand better the rather complex spatial, kinematic and excitation structure in the FELs of TTSs we have carried out a long-slit spectroscopic survey of 38 TTSs. Our study significantly increases the number of TTSs with available long-slit data and allows statistically more significant conclusions on the spatial properties of the FEL regions. As previously pointed out by one of us (e.g. Solf 1989) long-slit spectroscopy is a rather powerful method to obtain information on the small-scale ($\leq 1'' - 2''$) structure of the FELs even on subarcsec (subseeing) scales because it is a differential method using the bright stellar continuum as a spatial reference (see also below).

Our paper is structured as follows: In Sect. 2 we outline the observations and the data reduction. In Sect. 3 we describe the results of the 9 most detailly investigated TTSs. In Sect. 4 the results of our survey are summarized and discussed.

2. Observations and data reduction

For our long-slit spectroscopic survey of the FELs of TTSs we have selected a total of 38 objects which cover a wide range of equivalent widths of the [OI] λ6300 line in the catalogue of Cohen & Kuhi (1979).

Table 1. List of observing periods at the Calar Alto Observatory (CA) and the Observatorio Roque de los Muchachos (WHT). (c = 2.2 m coudé spectrograph, T = 3.5 m Cassegrain twin spectrograph, I = 4.2 m ISIS Cassegrain spectrograph)

campaign	telescope	period	instrument
1	CA 3.5 m	02.12.88 – 10.12.88	T
2	CA 3.5 m	14.12.88 – 22.12.88	T
3	CA 2.2 m	07.09.92 – 16.09.92	c
4	CA 3.5 m	14.12.92 – 21.12.92	T
5	CA 2.2 m	14.12.92 – 21.12.92	c
6	CA 2.2 m	24.08.93 – 30.08.93	c
7	WHT 4.2 m	31.08.93 – 05.09.93	I
8	CA 2.2 m	01.09.93 – 30.09.93	c
9	CA 3.5 m	17.11.93 – 21.11.93	T

For many of these objects we have have taken long-slit spectra at various (usually 4-5) position angles. Note that for several TTSs of our sample spectrograms at only one position angle have been secured either because the outflow direction was known from imaging studies or because the spectrogram served only as a pre-investigation for possible future studies. The data were collected during several observing runs between 1988 and 1993 using the coudé spectrograph at the 2.2 m telescope and the Cassegrain twin spectrograph at the 3.5 m telescope of the Calar Alto (CA) Observatory in Spain. The spectral resolution was 20 km s^{-1} and 50 km s^{-1}, respectively. The spatial resolution, determined from the spatial width of the stellar continuum (FWHM$_c$), varied in general between 1.4″ and 2.0″. In 1993 we used, in addition, the ISIS spectrograph on the 4.2 m William Herschel Telescope (WHT) providing a spectral and spatial resolution of 35 km s^{-1} and $1'' - 1.3''$, respectively. The wavelength coverage at the WHT and CA 3.5 m telescope was from 6250 to 6750 Å. At the CA 2.2 m telescope the wavelength coverage was

from 6250 to 6450 Å or from 6535 to 6735 Å per frame. The individual observing periods are listed in Table 1.

The spectra were reduced by a program developed by one of us (J.S.). Following the standard data reduction, a special continuum subtraction procedure was performed in order to reveal the relatively weak FEL regions near the source. This step is essential for deriving information about the spatial and kinematic properties of the outflow in the immediate vicinity of the YSO and is discussed in full detail elsewhere (Hirth et al. 1994a).

From the continuum-subtracted long-slit spectrograms position-velocity (PV) maps of the individual FELs have been derived. From these PV maps two important spatial quantities of the FELs as a function of the radial velocity have been extracted: the corrected spatial width Δy_0 ($\mathrm{FWHM_0}$) and the offset y of the position of the FEL centroid relative to the stellar position.

In a first step using the stellar continuum spectrum recorded on the original spectrogram the stellar position y_c and the actual spatial resolution Δy_c ($\mathrm{FWHM_c}$) have been derived by means of a Gaussian line fit in the spatial direction of the stellar continuum in the immediate vicinity of the FELs (i.e. along the direction of the slit). In a second step, using the recorded FELs on the continuum-subtracted long-slit spectrogram, the spatially integrated intensity I[1], the centroid position y', and the (uncorrected) spatial width Δy (FWHM) of the FEL distribution along the direction of the slit have been derived as a function of radial velocity by means of a Gaussian line fit to the FEL distribution recorded in each wavelength bin. Finally the spatial offset of the centroid $y = y' - y_\mathrm{c}$ and the corrected spatial width of the FEL Δy_0 ($\mathrm{FWHM_0}$) $= (\Delta y^2 - \Delta y_\mathrm{c}^2)^{0.5}$ as a function of radial velocity have been calculated. Due to the differential nature of that procedure a relatively high accuracy of the offset y of $\approx 0.05'' - 0.1''$ has been generally achieved. Evidently, due to the deconvolution procedure applied, the deduced spatial widths Δy_0 are of lower accuracy. Depending on the S/N ratio of the data in our spectrograms, reliable corrected spatial widths Δy_0 can only be deduced for Δy_0 larger than $0.2 - 0.3\ \Delta y_\mathrm{c}$. This means that $\Delta y_0 > 0.2...0.3\ \Delta y_\mathrm{c}$ is required to deduce reliable changes in Δy_0 as a function of radial velocity (e.g. the differences between the LVC and HVC). Although our method is relatively sensitive to derive relative changes in the spatial width the absolute values for the corrected width Δy_0 may be systematically wrong due to the assumption of Gaussian profiles for both the emission region and the point spread function.

The outflow direction has been determined by comparing long-slit spectra centered on the star and obtained at different position angles in steps of 20° to 30°. Spectra taken with a slit orientation parallel to the outflow show the maximum spatial offset of the emission centroid of the FEL from the stellar position (for more details see Hirth et al. 1994a). Spectra taken perpendicular to the determined outflow direction show no significant spatial offset of the FEL (i.e. less than $0.05'' - 0.1''$). This is an important criterion for the validity of the determined outflow direction. Of course, there are several cases in which the outflow direction was known already from direct imaging in the [SII] $\lambda\lambda$6716, 6731 lines or in Hα.

The kinematical properties of the forbidden line emission were derived by Gaussian fits in the PV maps along the radial velocity axis. The typical error in radial velocity space was ≈ 5 km s^{-1} for the Cassegrain twin and ISIS spectra and ≈ 2 km s^{-1} for the coudé spectra. The velocity width Δv_0 (FWHM) of the individual components of the FEL was again determined by quadratic subtraction of the instrumental profile Δv_i (FWHM) from the measured width Δv (FWHM), i.e. $\Delta v_0 = (\Delta v^2 - \Delta v_i^2)^{0.5}$.

3. Results of individual objects

In the following we discuss in detail the long-slit spectra of the 9 TTSs (Haro 6-10, XZ Tau, UZ Tau E, HN Tau, DO Tau, DP Tau, UY Aur, RW Aur and V536 Aql) for which the most detailed information is available on the spatial distribution of the FEL regions in the lines of [OI] $\lambda\lambda$6300, 6363, [NII] λ6583 and the [SII] $\lambda\lambda$6716, 6731 and also on the outflow direction. In the latter case long-slit spectra at sufficiently large number of orientations have been taken to determine the unknown outflow direction (see also Hirth et al. 1994a), unless the outflow direction is known from narrow-band imaging. First results on DO Tau, DP Tau and RW Aur have been briefly discussed elsewhere (Hirth et al. 1994b). A detailed discussion of the data for CW Tau is given in Hirth et al. (1994a). The following examples also give the reader an idea of the sometimes rather complex spatial and kinematic structure of the FEL region of the investigated TTSs and the often strong differences between individual objects.

3.1. Haro 6-10

Haro 6-10 (HH 184) is an embedded TTS with strong FELs surrounded by a small nebula consisting of a mixture of HH emission and scattered continuum light. It has a deeply embedded IR companion which is much fainter at H and K than at L and M (Seperation $2''$, $\Delta K = 2.2$ mag, PA = 355°; Leinert & Haas 1989). More details about previous studies are given in Strom et al. (1986), Leinert & Haas (1989) and Reipurth (1994). Direct images of Haro 6-10 presented by Elias (1978) and Strom et al. (1986) show a HH knot some $50''$ southeast from the source at PA = 247° and a much fainter and extended feature at about $170''$ distance at PA = 232°. On the basis of these images we assumed that the outflow is oriented at around PA = 240° and placed the slit at PA = 247° through Haro 6-10 and the HH knot. Note that spatial and kinematic data derived from spectra of the FELs have not been available before our survey.

[1] The spatially integrated intensity is proportional to the peak intensity of the Gauss fit and its spatial width at FWHM.

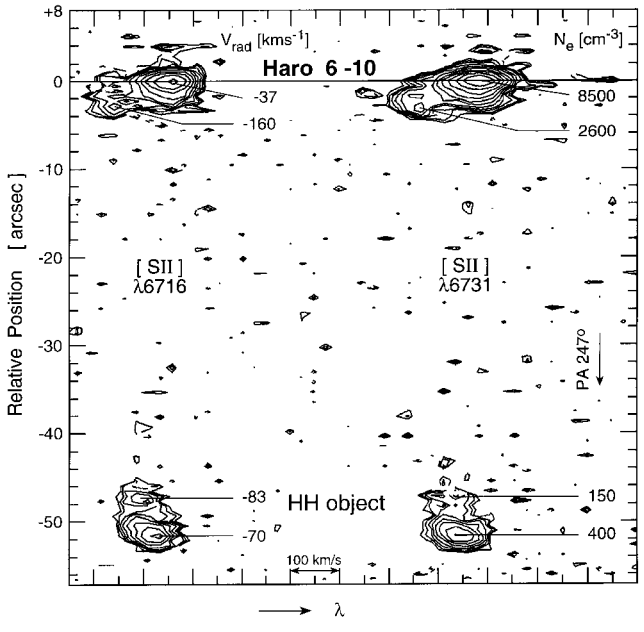

Fig. 1. Position-velocity map of the [SII] λ6716 and [SII] λ6731 lines of Haro 6-10 and its associated HH object extracted from data taken with the 3.5 m Cassegrain twin spectrograph in December 1988 (PA = 247°). The stellar continuum has been subtracted. The spacing of the contours is logarithmic corresponding to a factor $2^{0.5}$ in the intensity. Relative positions and velocities are quoted with respect to the stellar position and stellar velocity, respectively. On the right hand side the electron densities of various emission line features are given

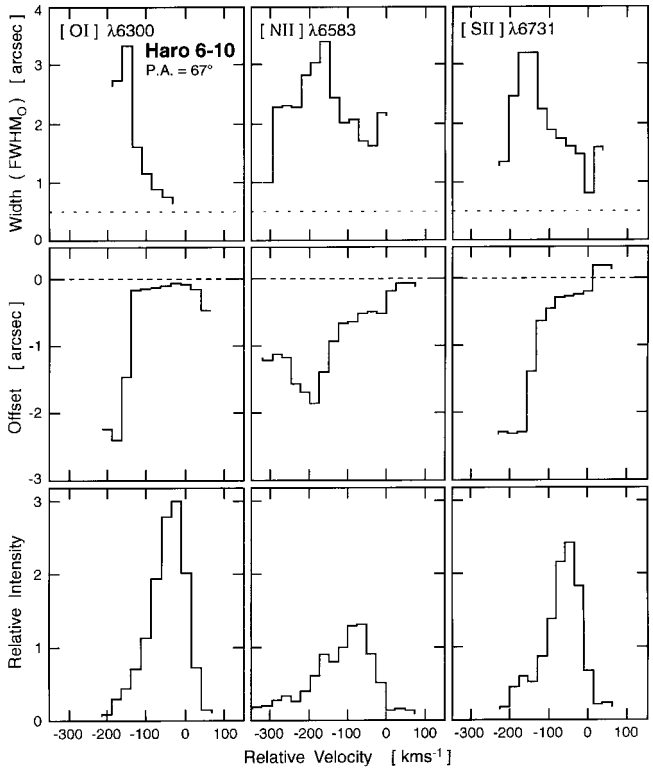

Fig. 2. Spatial width (top part), spatial offset (middle part) and spatially integrated intensity (lower part) of the [OI] λ6300, [NII] λ6583 and [SII] λ6731 line emission of Haro 6-10 as a function of the radial velocity (PA = 247°). The dotted line in the plots of the spatial width indicates the lower limit for which changes in width with velocity can be reliably measured. The radial velocity has been measured relative to the stellar velocity. The data are extracted in part from the continuum-subtracted position-velocity map displayed in Fig. 1

The long-slit spectra of Haro 6-10 were obtained with the 3.5 m Cassegrain twin spectrograph in December 1988. From the PV map shown in Fig. 1 one clearly sees that in the [SII] $\lambda\lambda$6716, 6731 lines the emission region is spatially extended along PA = 247°. The FELs of the above mentioned HH knot have been detected as well, permitting us to deduce its kinematic properties for the first time. The radial velocities at 47″ and at 52″ distance from the outflow source are -83 km s^{-1} and -70 km s^{-1}, respectively. The electron densitites derived for this HH knot ($150 - 400$ cm^{-3}) are relatively low compared to the values for the emission near the stellar position (8500 cm^{-3}). Note that for the highly blueshifted gas at -160 km s^{-1} lower electron densities were derived (2600 cm^{-3}) compared to the values of 8500 cm^{-3} for the peak emission at -37 km s^{-1}.

Details about the kinematic and spatial properties of the FEL region of Haro 6-10 are shown in Fig. 2. The plots display the spatial width Δy_0 (FWHM$_0$), the offset y and the spatially integrated intensity I as a function of the radial velocity with respect to the stellar velocity. All quantities are derived by a Gaussian line fit over the FEL region in spatial direction of the continuum-subtracted spectrogram as described in Sect. 2.

The [OI] λ6300, [NII] λ6583 and the [SII] λ6731 lines show line emission over a very broad range of velocities with blue wings extending up to -300 km s^{-1} in [NII] λ6583. However, a well separated LVC and HVC is not evident in the line profiles of [OI] λ6300 and [SII] λ6731 like for example in V536 Aql (see Figs. 20 and 21).

Among the studied FELs the [NII] λ6583 line is the best diagnostic tool for the investigation of the HVC (or the high-velocity gas in general), since to our knowledge this line never forms a LVC. The [NII] λ6583 line peaks at ≈ -80 km s^{-1} and we therefore assume a radial velocity of -80 km s^{-1} for the HVC, which is in line with the velocity of the HH object. Therefore the broad emission peak of the [OI] and [SII] lines at ≈ -40 km s^{-1} probably represents the blend from both a LVC and a HVC where the LVC is more spatially compact. Such a blended LVC and HVC would also explain why the offset and spatial width in the [SII] and [OI] lines is slowly but systematically increasing between 0 and -100 km s^{-1}. At velocities between -120 to -200 km s^{-1} the offset in the [OI] λ6300 and [SII] λ6731 lines increases strongly and reaches values of about 2″ in both lines at velocities of -200 km s^{-1}. Although for these high velocities no significant differences between the

spatial properties of the [OI] λ6300 and [SII] λ6731 lines are detected this is not the case at low velocities where the offset and spatial width of the peak emission of the [SII] λ6731 line are nearly as twice as large as the corresponding values for the [OI] λ6300 line. In the [NII] λ6583 line the offset of the line emission is even higher around the peak of the emission when comparing with the [OI] λ6300 and [SII] λ6731 lines. A similar trend has been observed for several other TTSs (see Sect. 4.1 below).

We finally like to note that it is rather unclear why the gas at radial velocities of about -200 km s^{-1} has such a large offset and why it has so much higher radial velocities than the HH object or the HVC (i.e. the peak of the [NII] emission). Maybe there was a phase of much higher outflow velocities in the past. It is also possible that we observe an independent HVC from the companion of Haro 6-10.

3.2. XZ Tau

XZ Tau is a double star. The two components are separated by about 0.3″ in PA = 154° and differ in K-magnitude by about a factor of 3 (Leinert et al. 1993). Profiles of the FELs have first been published by Appenzeller et al. (1984). Deep [SII] $\lambda\lambda$6716, 6731 CCD images of XZ Tau were first published by Mundt et al. (1988) and Mundt et al. (1990). These authors show that XZ Tau is associated with a bipolar outflow with a PA $\approx$ 15° for the blueshifted part of the flow. Because of the low luminosity of the binary component XZ Tau B, the component A is more likely the source of the outflow. Previous long-slit spectra of the FELs of XZ Tau have been discussed by Solf (1989) and Mundt et al. (1990).

Since the ouflow direction at PA $\approx$ 15° is known from CCD imaging we have taken deep long-slit spectrograms only close to this position angle at PA = 19°. PV maps of the [OI] λ6300 line, [NII] λ6583 and [SII] λ6731 lines of XZ Tau derived from these long-slit spectra are shown in Fig. 3. In the [NII] λ6583 line the very broad red emission is rather prominent.

The spatial and kinematical properties of the bipolar outflow are shown in more detail in Fig. 4. Note that due to the spectral resolution of about 50 km s^{-1} in the Cassegrain twin spectra the line profiles of the [OI] λ6300 and [SII] λ6731 line are not resolved into a LVC and HVC. However, data from coudé spectra with a higher spectral resolution clearly show a double-peaked line profile with a HVC at -70 km s^{-1} in the [SII] λ6731 line and -54 km s^{-1} in the [OI] λ6300 line, and with a LVC at -7 km s^{-1} and $+4$ km s^{-1}, respectively (see Figs. 22f and g).

The bipolarity of the outflow is most clearly evident in the [NII] λ6583 line by the corresponding changes in the sign of the offset. In most other TTSs of our sample the offset (and often the spatial width) is largest in the [NII] λ6583 line and smallest in the [OI] λ6300 line. For XZ Tau this is the case for the blueshifted part of the bipolar outflow but not for the redshifted part where similar values in [SII] and [NII] are observed.

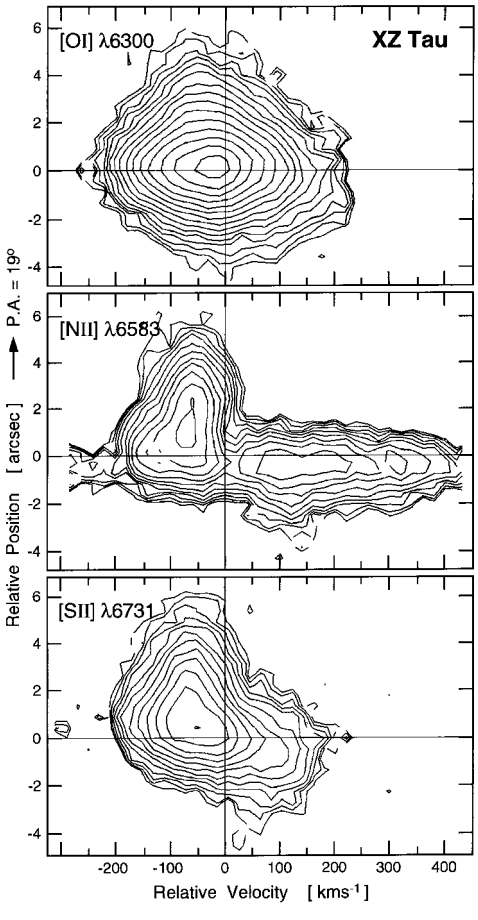

Fig. 3. Position-velocity maps of the [OI] λ6300, [NII] λ6583 and [SII] λ6731 lines of of XZ Tau extracted from data taken with the 3.5 m Cassegrain twin spectrograph in November 1993 (PA = 19°). The stellar continuum has been subtracted. Contours, positions and velocities as in Fig. 1

Like in many other TTSs studied here, the spatial width for the HVC is much larger in the [NII] λ6583 and [SII] λ6731 lines than in the [OI] λ6300 line. In the [NII] λ6583 line the spatial width is $\approx$ 4″ for the blueshifted part while the corresponding value for the [OI] λ6300 line is only $\approx$ 1″. In the velocity range of the LVC of the [OI] λ6300 and [SII] λ6731 lines one recognizes a local minumum in the spatial width. This trend is already expected from previous studies (e.g. CW Tau in Hirth et al. 1994a) where the LVC shows a smaller offset and spatial width than the HVC.

3.3. UZ Tau E

Observations of the [OI] λ6300 line of UZ Tau E were first discussed in Appenzeller et al. (1984). They detected a LVC and a broad HVC. Recent data on the FELs of this TTS have been published by Hartigan et al. (1995).

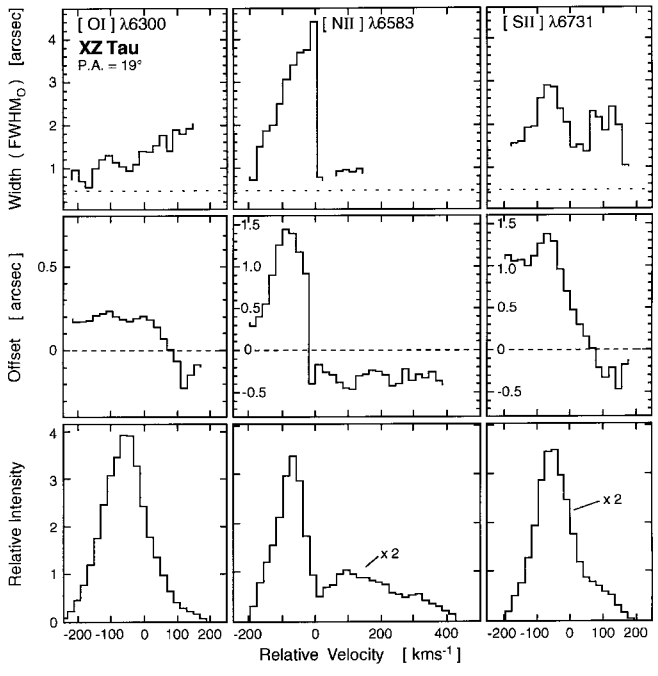

Fig. 4. Spatial width (top part), spatial offset (middle part) and spatially integrated intensity (lower part) of the [OI] λ6300, [NII] λ6583 and [SII] λ6731 line emission of XZ Tau as a function of the radial velocity (PA = 19°). The dotted line in the plots of the spatial width indicates the lower limit for which changes in width with velocity can be reliably measured. The radial velocity has been measured relative to the stellar velocity. The data are extracted from the continuum-subtracted position-velocity maps displayed in Fig. 3

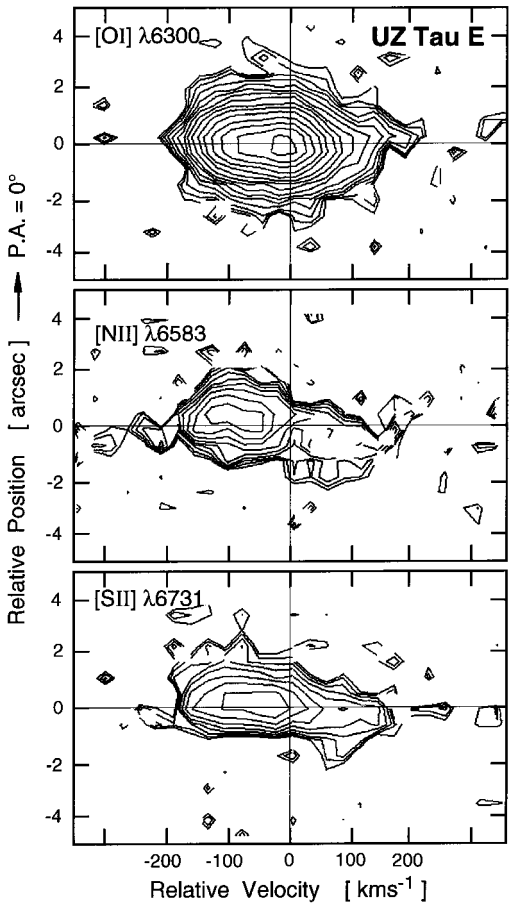

Fig. 5. Position-velocity maps of the [OI] λ6300, [NII] λ6583 and [SII] λ6731 lines of UZ Tau E extracted from data taken with the 3.5 m Cassegrain twin spectrograph in December 1988 (PA = 0°). The stellar continuum has been subtracted. Contours, positions and velocities as in Fig. 1

Information on the spatial properties of the FELs of UZ Tau E is so far not available.

Long-slit spectra of UZ Tau E have been taken at four position angles (PA = 0°, 45°, 90° and 315°). Since we have found evidence for a bipolar outflow only in our north-south oriented slit, as illustrated in Fig. 5, we believe that the blueshifted part of the bipolar outflow is roughly oriented towards PA = 0°. The PV maps in Fig. 5 show that the bipolar nature of the outflow is most clearly evident in the [NII] λ6583 line. This is further illustrated in Fig. 6 where more details about the kinematic and spatial properties of the FELs are displayed. From this figure it is evident, that the bipolar outflow is also indicated in the [OI] λ6300 line but the offsets are half as large as in the [SII] λ6731 line. In the plots of the spatial width versus radial velocity (see Fig. 6) one can recognize that in the [OI] λ6300 and [SII] λ6731 lines the spatial width is smallest around the stellar velocity. As already mentioned above, this behaviour is also observed in other TTSs in our sample.

The [OI] λ6300 and [SII] λ6731 lines do not show a pronounced double-peaked line profile, presumably due to the moderate spectral resolution of the Cassegrain twin spectra (≈ 50 km s^{-1}). However, it is known from high-resolution spectroscopic studies (see Appenzeller et al. 1984 and Hartigan et al. 1995) that both a HVC and a LVC exist at velocities of −90 and 0 km s^{-1}, respectively. From a two-component Gaussian fit to our [OI] λ6300 data we derive a radial velocity of −107 km s^{-1} for the HVC and −10 km s^{-1} for the LVC. For the [SII] λ6731 line the corresponding values are −103 km s^{-1} and −11 km s^{-1}, respectively. For the [NII] λ6583 line only a HVC at −86 km s^{-1} has been detected. For the redshifted part of the bipolar outflow no distinct HVC is evident in the line intensity profile shown in Fig. 6. But the broad redshifted wing reaches to velocities of about +150 km s^{-1} in all lines. Note that in the spectra of Hartigan et al. (1995) one can see the redshifted emission in both the [OI] λ6300 and [SII] λ6731 lines at similar radial velocities.

Jensen et al. (1996) have argued on the basis of their ^{12}CO 2 − 1 observations that UZ Tau is sourrounded by a disk with the disk plane being oriented at about PA ≈ 19°, i.e., approximataly at our derived outflow direction. They furthermore argue that such a disk orientation is strongly

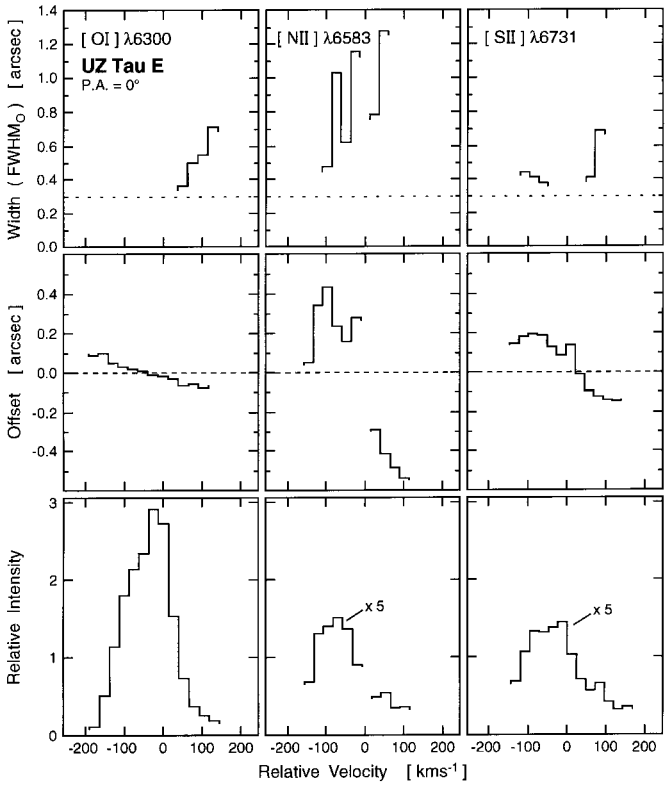

Fig. 6. Spatial width (top part), spatial offset (middle part) and spatially integrated intensity (lower part) of the [OI] λ6300, [NII] λ6583 and [SII] λ6731 line emission of UZ Tau E as a function of the radial velocity (PA = 0°). The dotted line in the plots of the spatial width indicates the lower limit for which changes in width with velocity can be reliably measured. The radial velocity has been measured relative to the stellar velocity. The data are extracted from the continuum-subtracted position-velocity maps displayed in Fig. 5

supported by the measured position angles of the electric polarization vector which often has a similar orientation as the disk plane (see e.g. Bastien 1989). This result clearly contradicts our derived disk orientation of about PA = 90° (assuming that the disk is oriented perpendicular to the bipolar outflow). We suggest that the ^{12}CO 2 − 1 data of Jensen et al. (1996) can also be explained by a bipolar outflow and that there is no convincing argument that their data can only be interpreted by disk rotation. Furthermore the available polarization data are not useful to argue for a certain disk orientation, since in these polarization studies the combined light of both UZ Tau E and W has been measured. In summary we believe that the ^{12}CO 2−1 data of Jensen et al. (1996) and our data can be understood, if the blueshifted part of the outflow from UZ Tau E is oriented at PA ≈ 20°.

3.4. HN Tau

HN Tau is one of the TTSs in our sample with the strongest forbidden line emission ($W_\lambda \approx 14$ Å for the [OI] λ6300 line) and has therefore been selected for our studies. Previous high-resolution [OI] and [SII] line profiles of this star published by Edwards et al. (1987) and Hartigan et al. (1995) do not show a double-peaked line profile as observed for other TTSs but only display a very broad blueshifted emission with a weak red wing in [OI] λ6300. First long-slit spectra were discussed by Solf (1989).

With the 3.5 m Cassegrain twin spectrograph we have taken long-slit spectra at PA = 0°, 45°, 90° and 270°. Furthermore we have obtained two high-resolution coudé spectrograms at PA = 70° and 340°. From the observed offset of the high-velocity emission in these spectra we conclude that the blueshifted part of the outflow is oriented between PA = 340° and 0°.

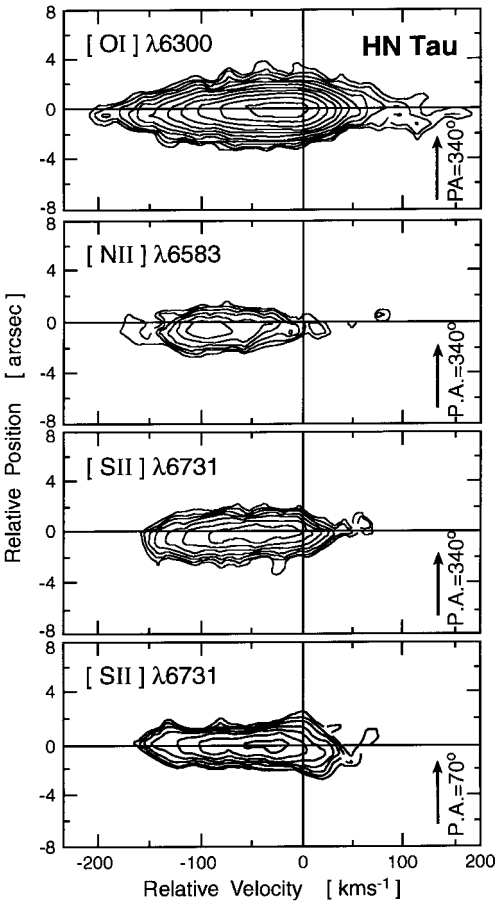

Fig. 7. Position-velocity maps of the [OI] λ6300, [NII] λ6583 and [SII] λ6731 lines of HN Tau extracted from data taken with the 2.2 m coudé spectrograph in September 1992 (PA = 70° and 340°). The stellar continuum has been subtracted. Contours, positions and velocities as in Fig. 1

Figure 7 shows the PV diagrams of the [OI] λ6300, [NII] λ6583 and the [SII] λ6731 lines at PA = 340° derived from the coudé spectra. For comparison the PV diagram of the [SII] λ6731 line at PA = 70° is also shown. The PV maps of the [OI] λ6300 and the [SII] λ6731 lines at PA = 340° clearly illustrate the increase of the offset with

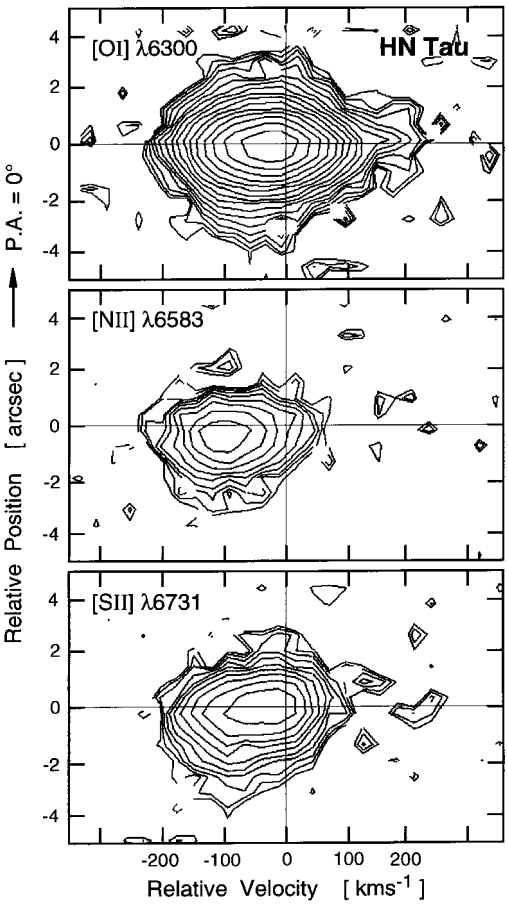

Fig. 8. Position-velocity maps of the [OI] λ6300, [NII] λ6583 and [SII] λ6731 lines of HN Tau extracted from data taken with the 3.5 m Cassegrain twin spectrograph in December 1988 (PA = 0°). The stellar continuum has been subtracted. Contours, positions and velocities as in Fig. 1

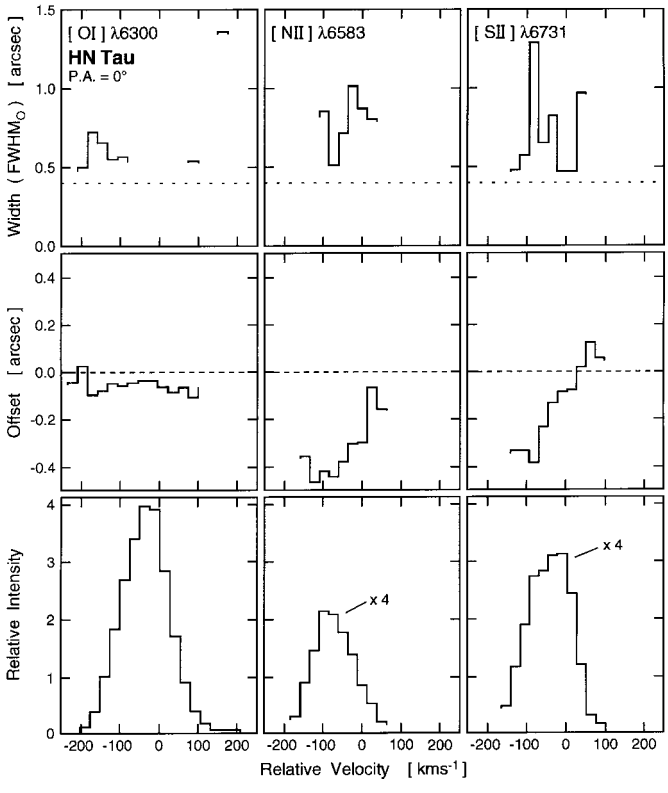

Fig. 9. Spatial width (top part), spatial offset (middle part) and spatially integrated intensity (lower part) of the [OI] λ6300, [NII] λ6583 and [SII] λ6731 line emission of HN Tau as a function of the radial velocity (PA = 0°). The dotted line in the plots of the spatial width indicates the lower limit for which changes in width with velocity can be reliably measured. The radial velocity has been measured relative to the stellar velocity. The data are extracted from the continuum-subtracted position-velocity maps displayed in Fig. 8

increasing blueshift of the emission. The PV diagram of the [SII] λ6731 line at PA = 70° shows, as expected, that there is no significant offset at a position angle approximately perpendicular to the outflow direction.

Due to their lower spectral resolution the PV maps of the [OI] λ6300, [NII] λ6583 and the [SII] λ6731 lines derived from the Cassegrain twin spectrograms do not clearly show the increase of the offset with increasing velocity (see Fig. 8). But the effect is evident in the [NII] λ6583 and the [SII] λ6731 lines as better illustrated in Fig. 9. The offsets of the [SII] line plotted seems to suggest a bipolar outflow, since the redshifted parts of the emission has apparently positive offsets. However, such a bipolar outflow is not supported by the nearly constant offset measured in the [OI] λ6300 line (see Fig. 9) and by the PV map of the [SII] λ6731 line shown in Fig. 7.

A comparison of the line intensity profiles shown in Fig. 9 and Fig. 22h shows that the [NII] line peaks at much larger negative radial velocities than the [OI] lines (-86 km s^{-1} as compared to -30 km s^{-1}, see also Fig. 7).

It is known that the [NII] line in TTSs shows normally no LVC (see also Sect. 4). Therefore the lower radial velocity of the [OI] line can be explained by a strong LVC in that line which is spectroscopically unresolved from the HVC due to the large internal velocity widths of both components. In the [SII] lines a LVC is probably also present. The existence of a LVC in both the [OI] and [SII] lines is also consistent with the smaller offsets and smaller spatial widths observed at velocities between -30 km s^{-1} and 0 km s^{-1} (see Fig. 7 and Fig. 9).

3.5. DO Tau

DO Tau is a classical TTS (CTTS) associated with an arc-like reflection nebula (see POSS). Profiles of FELs have first been published by Appenzeller et al. (1984) and Edwards et al. (1987). First results on the spatial properties of the FELs, based on long-slit spectra obtained with the Cassegrain twin spectrograph, have been discussed by Hirth et al. (1994b).

Spectrograms have been taken at seven different slit positions in December 1988 (PA = 15°, 50°, 70°, 80°,

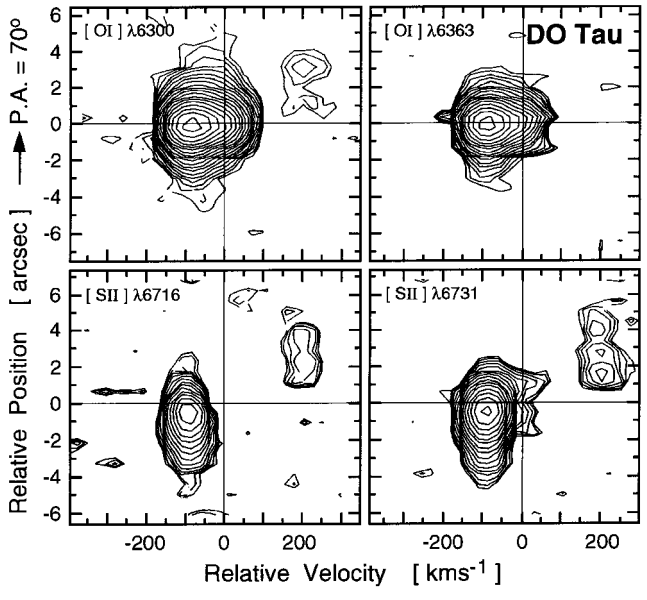

Fig. 10. Position-velocity maps of the [OI] λ6300, [OI] λ6363, [SII] λ6716 and [SII] λ6731 lines of DO Tau extracted from data taken with the 3.5 m Cassegrain twin spectrograph in December 1988 (PA = 70°). The stellar continuum has been subtracted. Contours, positions and velocities as in Fig. 1

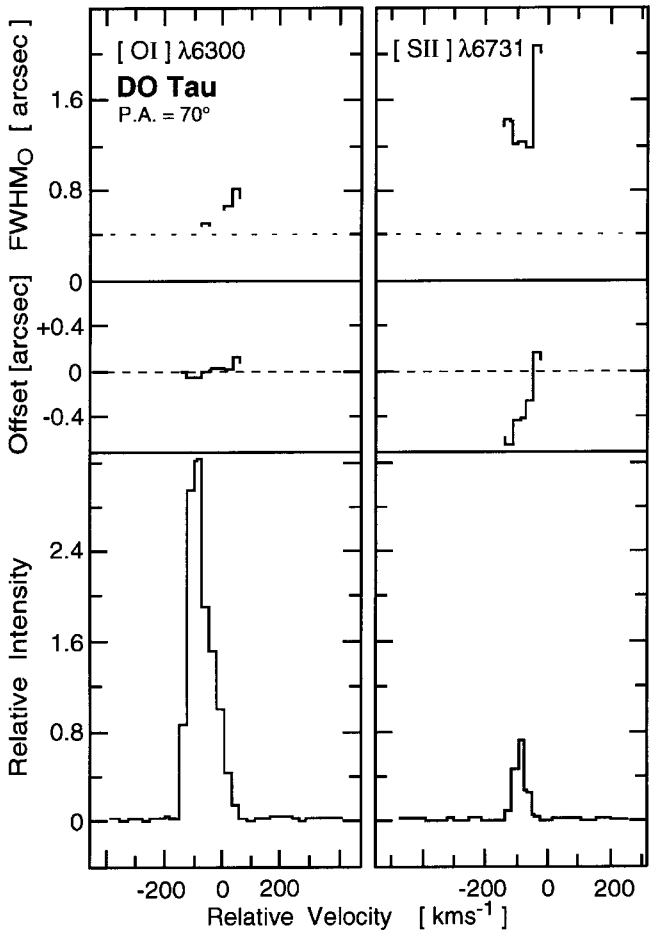

Fig. 11. Spatial width (top part), spatial offset (middle part) and spatially integrated intensity (lower part) of the [OI] λ6300 and [SII] λ6731 line emission of DO Tau as a function of the radial velocity (PA = 70°). The dotted line in the plots of the spatial width indicates the lower limit for which changes in width with velocity can be reliably measured. The radial velocity has been measured relative to the stellar velocity. The data are extracted from the corresponding continuum-subtracted position-velocity maps displayed in Fig. 10

110°, 160° and 285°). They show the existence of a bipolar outflow with the blueshifted part being oriented at PA = $250 \pm 10°$. Note that the determined outflow direction is nearly perpendicular to the polarization angle of $175 \pm 2°$ found by Bastien (1985).

The outflow is detected in the [SII] $\lambda\lambda$6716, 6731 and in the [OI] $\lambda\lambda$6300, 6363 lines but neither in Hα nor in the [NII] $\lambda\lambda$6548, 6583 lines.

PV maps of the [OI] $\lambda\lambda$6300, 6363 and the [SII] $\lambda\lambda$6716, 6731 lines are shown in Fig. 10. These diagrams show that DO Tau has a bipolar outflow, with the blueshifted part being much more prominent than the redshifted one. The bipolar outflow extends up to 4″ from the star and, like in the case of RW Aur (Hirth et al. 1994b), shows asymmetries both in morphology and kinematics on either side of the star. In particular, in the [SII] lines the blueshifted part of the outflow shows radial velocities of -92 km s^{-1} at 1.5″ distance from the star, whereas, at the same position in the redshifted part of the outflow, the corresponding value is $+210$ km s^{-1}.

We note that, in contrast to the blueshifted part, the redshifted part of the outflow can not be continously traced back to the stellar position. This is probably due to the existence of a circumstellar disk occulting the redshifted emission near the star, unless the gap in redshifted emission is due to an intrinsic faintness because of unfavourable excitation conditions.

In the blueshifted part of the outflow the HVC shows different kinematic properties in the [OI] λ6300 and [SII] λ6731 lines. Compared to the [SII] line the radial velocities in the [OI] line is lower by 10 to 15 km s^{-1}. Furthermore, the velocity dispersion in the [OI] lines is about two times larger than in the [SII] lines. This might be the result of an increasing jet collimation with increasing distance from the outflow source, as discussed in Mundt & Hirth (1997).

High resolution line profiles of the [OI] λ6300 and [SII] λ6731 lines of DO Tau are shown in Fig. 22i. These data are extracted from coudé spectra which have a 2.5 times higher spectral resolution compared to the deep 3.5 m Cassegrain twin spectrograph data shown in Fig. 11. The higher spectral resolution of the coudé spectra probably explains why we observed a double-peaked line profile in the [OI] lines, i.e. a HVC and a LVC. In the [SII] lines only a HVC has been found. However, the emission in the red wing of the HVC in the [SII] lines (between -80 km s^{-1} and 0 km s^{-1}) might indicate the existence of a very weak

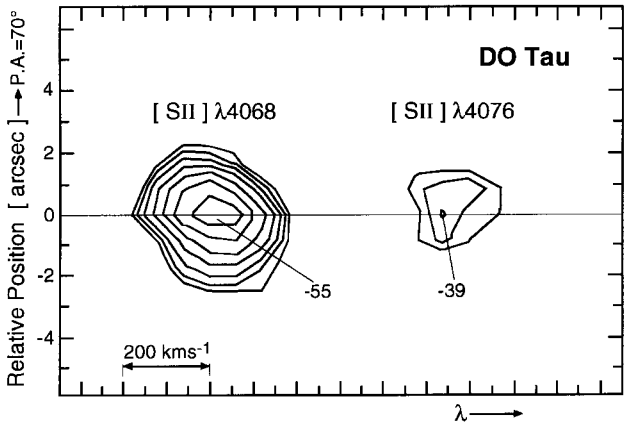

Fig. 12. Position-velocity maps of the [SII] $\lambda\lambda$4068, 4076 lines of DO Tau extracted from data obtained with the blue channel of the 3.5 m Cassegrain twin spectrograph in December 1992 (PA = 70°). Contours, positions and velocities as in Fig. 1

LVC (see Fig. 22i). Note that, contrary to the case of the Cassegrain twin spectra, the redshifted part of the outflow could not be detected in the coudé spectra due to the relatively low S/N ratio. We like to mention that in most other TTSs the LVC is observed in [SII] too. The only other examples among our investigated stars where a LVC is only observed in [OI] and not in [SII] is FN Tau (see Fig. 22a) and RW Aur (see Sect. 3.8).

Figure 11 shows more details about the spatial characteristics of the bipolar outflow of DO Tau deduced from the PV diagrams shown in Fig. 10. (We again note that in these data a double-peaked line profile in the [OI] λ6300 line could not be resolved because of the lower spectral resolution). From Fig. 11 it is evident that the spatial offset and spatial width of the [SII] λ6731 line are much larger than the corresponding values of the [OI] λ6300 line, a result which was found for most other stars in our sample.

The data permit us to derive the electron densities (N_e) in both parts of the bipolar outflow. In the blueshifted part of the outflow N_e decreases from 3800 cm^{-3} to about 600 cm^{-3} between 2″ and 4″ distance from the star. At comparable distances in the redshifted part densities of about 5000 cm^{-3} have been derived but no significant spatial variation of the electron density has been detected between 2″ and 4″ distance from DO Tau.

In addition, we measured the [SII] λ6731/[OI] λ6300 line ratio in the blueshifted part of the outflow. This ratio increases from 0.2 at the stellar position up to 1.5 at 2″ distance from DO Tau. Further out the [OI] line flux decreases very fast making a determination of the [SII]/[OI] line ratio impossible. In the redshifted part of the outflow an increase of the line ratio from 1.3 to about 3.0 at distances between 2″ and 4″ has been detected. These values are comparable with those measured in HH objects and are in line with the results obtained for CW Tau (see Hirth et al. 1994a) and RW Aur (see below). In all these cases, the increase of the [SII]/[OI] line ratios with increasing distance from the source can most probably be explained by a corresponding decrease in electron density (see Sect. 3.8 and Mundt et al. 1990).

Furthermore the [SII] $\lambda\lambda$4068, 4076 lines of DO Tau have been observed with the blue channel of the 3.5 m Cassegrain twin spectrograph in December 1992 (see Fig. 12). Whereas the much fainter [SII] λ4076 line appeares spatially resolved, this is not the case for the [SII] λ4068 line. The equivalent width for the [SII] λ4068 line is -4.1 Å. The radial velocity relative to the star is -55 km s^{-1} and the velocity dispersion at FWHM is 167 km s^{-1}. However, the [SII] λ4068 line is heavily disturbed by Fe I λ4064 emission in the blue and Fe I λ4072 emission in the red wing. Therefore the values for the equivalent width and the velocity dispersion are quite uncertain. The same holds for the [SII] λ4076 line, which is disturbed by Sr II λ4078 emission in the red wing. The equivalent width for the [SII] λ4076 line is -1.2 Å. The radial velocity and velocity dispersion are -39 km s^{-1} and 150 km s^{-1}, respectively. Note the lower negative radial velocities and the much higher velocity dispersions of the short wavelength [SII] FELs compared to the [OI] $\lambda\lambda$6300, 6363 and [SII] $\lambda\lambda$6716, 6731 lines (cf. Table 2). Due to the relatively large velocity dispersion of the [SII] $\lambda\lambda$4068, 4076 lines and/or the large internal line width it is possible that we observe in these lines unresolved double-peaked line profiles. Data of higher spectral resolution of CW Tau and DG Tau show that a double-peaked line profile can also be present in the [SII] λ4068 line. In these two cases such a profile is observed also in the [SII] $\lambda\lambda$6716, 6731 lines (Hamann 1994). Note also that in the PV map of the [SII] λ4068 line a weak spatial gradient of the radial velocity in outflow direction is suggested. However, such a feature was not observed in the [SII] $\lambda\lambda$6716, 6731 lines (see Fig. 10).

3.6. DP Tau

DP Tau is a CTTS of spectral type M0 with strong line emission in [OI] λ6300 ($W_\lambda = 6.4$ Å; Cohen & Kuhi 1979).

First results of long-slit spectroscopic observations have been published in Hirth et al. (1994b). They have taken three long-slit spectrograms with the 4.2 m ISIS spectrograph of the WHT at position angles of PA = 20°, 42° and 60°. The orientations of the slit have been selected on the basis of a short exposure [SII] $\lambda\lambda$6716, 6731 image taken with the ISIS before the long-slit spectra. This image and the long-slit spectra suggest a PA of 222° for the blueshifted part of the bipolar outflow. This result has been recently confirmed by narrow-band images in the [SII] $\lambda\lambda$6716, 6731 lines obtained by Mundt & Eislöffel (1997). Their deep images clearly show a bipolar outflow at a PA of 41° and 221°.

Continuum-subtracted PV maps of the Hα, [NII] λ6583 and [SII] $\lambda\lambda$6716, 6731 lines have been published in Hirth et al. (1994b). Here we only show the PV maps of

the [OI] $\lambda\lambda$6300, 6363 and the [SII] $\lambda\lambda$6716, 6731 lines (see Fig. 13). As in the case of RW Aur and DO Tau, the asymmetric morphology of the bipolar outflow on either side of the star is obvious. As discussed in Hirth et al. (1994b) at distances larger than $5''$ from the star the Hα line shows different radial velocities in the redshifted and blueshifted part of the outflow: In the blueshifted part, velocities between -90 and -110 km s^{-1} are measured whereas at similar distances the redshifted part of the outflow shows a radial velocity of about $+30$ km s^{-1} only.

Due to the strong stellar Hα emission, the emission from the bipolar jets cannot be traced in Hα much closer to the star than about $2''-3''$. This is not the case for the lines of [OI] $\lambda\lambda$6300, 6363 and [SII] $\lambda\lambda$6716, 6731 shown in Fig. 13. A comparison of these lines with the Hα + [NII]λ6583 data in Fig. 3 of Hirth et al. (1994b) shows that the [SII] and [NII] data resemble each other. Therefore we will concentrate here on the comparison between the [SII] and [OI] lines shown in Fig. 13.

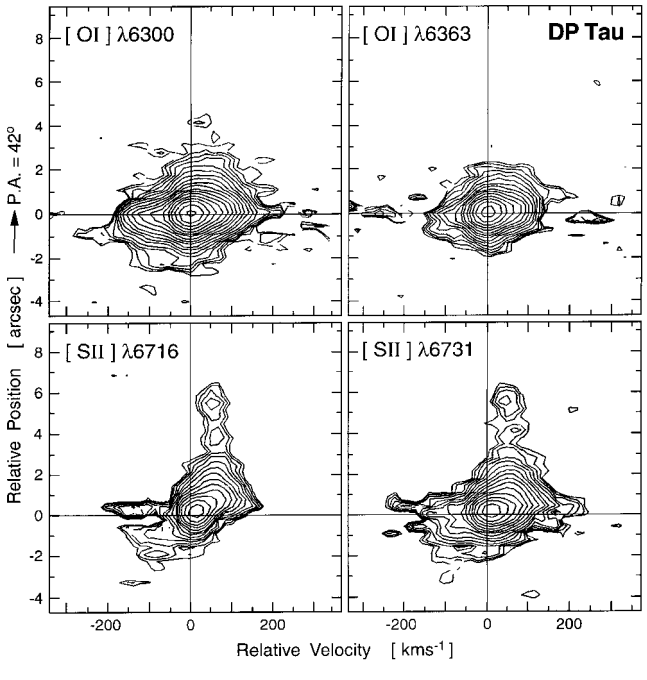

Fig. 13. Position-velocity maps of the [OI] λ6300, [OI] λ6363, [SII] λ6716 and [SII] λ6731 lines of DP Tau extracted from data taken with the 4.2 m ISIS Cassegrain spectrograph in September 1993 (PA = 42°). The stellar continuum has been subtracted. Contours, positions and velocities as in Fig. 1

The PV maps show significant differences between the [OI] and [SII] lines. These differences are presumably due to the higher density traced by the [OI] lines. Firstly, only the [OI] lines show the existence of a clear LVC with a radial velocity of -2 km s^{-1}. This component almost certainly represents a LVC since no significant offset and spatial width has been measured (see also the more detailed presentation of the spatial properties in Fig. 14).

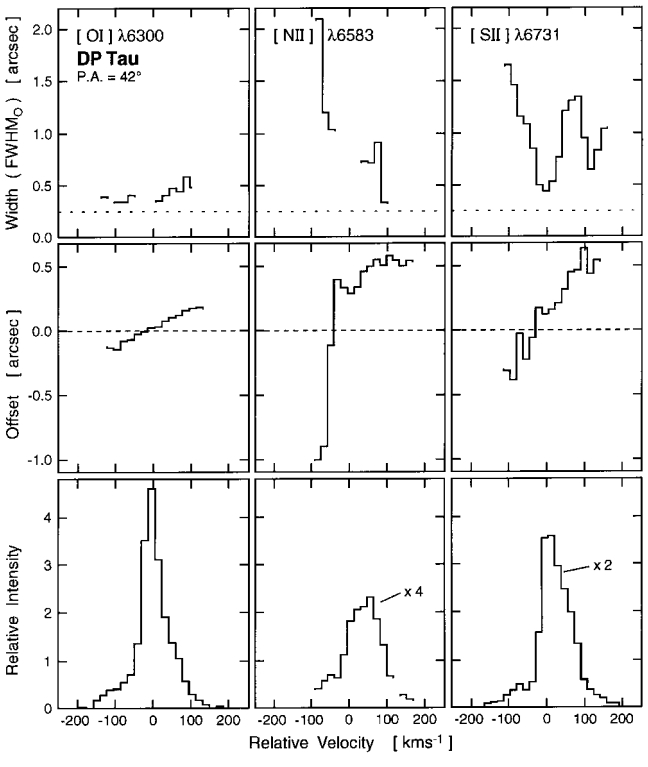

Fig. 14. Spatial width (top part), spatial offset (middle part) and spatially integrated intensity (lower part) of the [OI] λ6300, [NII] λ6583 and [SII] λ6731 line emission of DP Tau as a function of the radial velocity (PA = 42°). The dotted line in the plots of the spatial width indicates the lower limit for which changes in width with velocity can be reliably measured. The radial velocity has been measured relative to the stellar velocity. The data are extracted from the continuum-subtracted position-velocity maps displayed in Fig. 13

Furthermore in both the [SII] and [NII] lines no similar velocity component at the stellar velocity has been detected. We note that the component at about $+30$ km s^{-1} in the [SII] lines is most probably a redshifted HVC since it shows a relatively large offset of about $+0.2''$. Furthermore, a velocity component with similar spatial and kinematic characteristics is observed in the [NII] lines. However, it cannot be excluded, that in the [SII] line at low radial velocities we are observing a superposition of a faint LVC and the beginning of the high-velocity redshifted emission of the bipolar outflow. Similar to most other TTSs in our sample, Fig. 14 shows that the offset in [NII] λ6583 and [SII] λ6731 are much larger than in [OI] λ6300. The same trend is observed in the blueshifted part of the outflow for the spatial widths of these three FELs.

Note that although the spatial offset of the redshifted part of the outflow is similar in the [SII] λ6731 and [NII] λ6583 lines, the offset of the blueshifted part of the outflow is nearly twice as large in [NII] compared to [SII] (see Fig. 14). Such an asymmetry in the spatial properties of the bipolar outflow on either side of the star has been also

detected in V536 Aql and in the case of UZ Tau E for the [NII] λ6583 line.

Figures 13, 14 and 22j show that there is a prominent blue wing in the [OI] λ6300 line extending to velocities of ≈ -170 km s^{-1} (offset $\approx -0.2''$; see Fig. 14). The blue wing is relatively faint and diffuse in the [SII] λ6731 line and may be absent in the [SII] λ6716 line.

From the PV maps of the [NII] λ6583 and the [SII] lines it is also evident that the velocity asymmetries between the two parts of the bipolar outflow are already detectable at distances of about $1''$ from DP Tau. In particular on the blueshifted side in the [SII] lines one observes gas with velocities of -70 to -100 km s^{-1} while on the redshifted side velocities of $+30$ km s^{-1} are observed. The data on the redshifted side suggest in addition that strong velocity variations have taken place in the flow, e.g. at large distances from the star higher velocities ($\approx +60$ km s^{-1}) are observed than at smaller ditances ($\approx +30$ km s^{-1}). Also for the blueshifted side the Hα data of Hirth et al. (1994b) indicate variations in the outflow velocity. Furthermore it is interesting to note that in Hα the velocities of the redshifted flow (for distances $\geq 3''$) are half as small as the corresponding values in the [SII] and [NII] λ6583 lines. This latter result makes the whole situation rather confusing and suggests that in addition to a complex behaviour of velocity variations and asymmetries between the two sides of the outflow there may be some unusual excitation and density effects at work.

For the redshifted part of the outflow we have also determined the electron densities (N_e). This quantity decreases from the upper limit of the [SII] line method (≈ 30000 cm^{-3}) at the stellar position down to 3500 cm^{-3} at $0.8''$ distance from DP Tau and down to 750 cm^{-3} and 160 cm^{-3} at $4''$ and $5.5''$ distance further out. Furthermore, the [SII] λ6731/[OI] λ6300 line ratio increases from 0.4 at the stellar position up to 1.3 at $2''$. For the blueshifted part of the outflow the electron density N_e and the [SII]/[OI] line ratio have not been determined due to the low S/N ratio. As in the case of CW Tau (see Hirth et al. 1994a), RW Aur and DO Tau, these results imply that the density in the outflow is decreasing with increasing distance from the star (see also Sect. 3.8).

3.7. UY Aur

UY Aur is a binary. The components are separated $0.89''$ in PA = 255° and differ by about a factor of 1.5 in visual magnitude (Herbig & Bell 1988; Leinert et al. 1993). Cohen & Kuhi (1979) measured an equivalent width of the [OI] λ6300 line of -3.6 Å. Profiles of the FELs have been first published by Appenzeller et al. (1984), Edwards et al. (1987) and Hartigan et al. (1995).

Our long-slit spectrograms of UY Aur obtained at position angles of PA = 40°, 85°, 130° and 355° suggest the existence of a bipolar outflow at PA $\approx$ 40°.

Figure 15 shows the PV maps of UY Aur in the [OI] λ6300 and [SII] λ6731 lines at PA = 40° extracted from a spectrogram taken with the 3.5 m Cassegrain twin spectrograph in December 1988. Note that only a redshifted HVC at $+123$ km s^{-1} is visible in [SII] λ6731 whereas a blueshifted HVC has not been detected. However, in a Cassegrain twin spectrogram taken in December 1992 (not shown here) high-velocity blueshifted gas with velocities between -100 to -200 km s^{-1} is clearly evident in the [SII] λ6731 line profile.

The differences in the PV map between the [OI] λ6300 and [SII] λ6731 line are rather significant, with the [OI] λ6300 map showing a prominent emission extending up to -300 km s^{-1}. Why such an emission has not been detected in [SII] λ6731 in December 1988 is not fully understood. In part it could be due to the relatively low S/N ratio of the data and the relatively weak [SII] λ6731 flux. But certainly the physical conditions in the blueshifted part of the flow may also play a significant role. In particular, this part of the flow must be of relatively high density and low excitation in order to explain the strength of the [OI] λ6300 line and the absence of the [NII] λ6583 line. It would be also interesting to find out by further observations whether the velocity asymmetries observed by Hirth et al. (1994b) for many bipolar outflows from YSOs are also present in UY Aur. They could explain the smaller velocity extent of the [OI] λ6300 line in the redshifted side.

Further details about the kinematic and spatial properties of the [OI] λ6300 and [SII] λ6731 line emission regions are displayed in Fig. 16. Due to the medium resolution of the deep Cassegrain twin spectra no clear distinction between a HVC and a LVC is evident. From the change of the sign of the offset in the middle part of Fig. 16 the bipolar nature of the outflow is evident especially in the [OI] λ6300 line. As observed in many other TTSs, the offset of the (redshifted) HVC in the [SII] λ6731 line is larger than the HVC in the [OI] λ6300 line. However, note that the spatial width is similar for both lines.

The data extracted from our coudé spectrograms indicate further interesting details in the line profiles (see Fig. 22k). In the [OI] λ6300 line a broad redshifted wing with velocities extending up to $+180$ km s^{-1} is observed, while the blueshifted side of the emission extends up to -240 km s^{-1}. Furthermore the blueshifted part of the line profile indicates narrow peaks (FWHM < 50 km s^{-1}) at -85 km s^{-1}, -145 km s^{-1} and -205 km s^{-1}. Possibly, the data indicate multiple HVCs. In the [SII] λ6731 line no corresponding features have been detected.

3.8. RW Aur

The bright TTS RW Aur is a relatively isolated object (Herbig 1977). It is a hierachical triple system with the primary A having a separation of about $1.4''$ in PA = 256° from the close binary B&C (separation: $0.12''$; Ghez et al. 1993). The latter two components are about $2-3$ magnitudes fainter than the primary component. Profiles of the FELs of RW Aur have been first published by Hamann

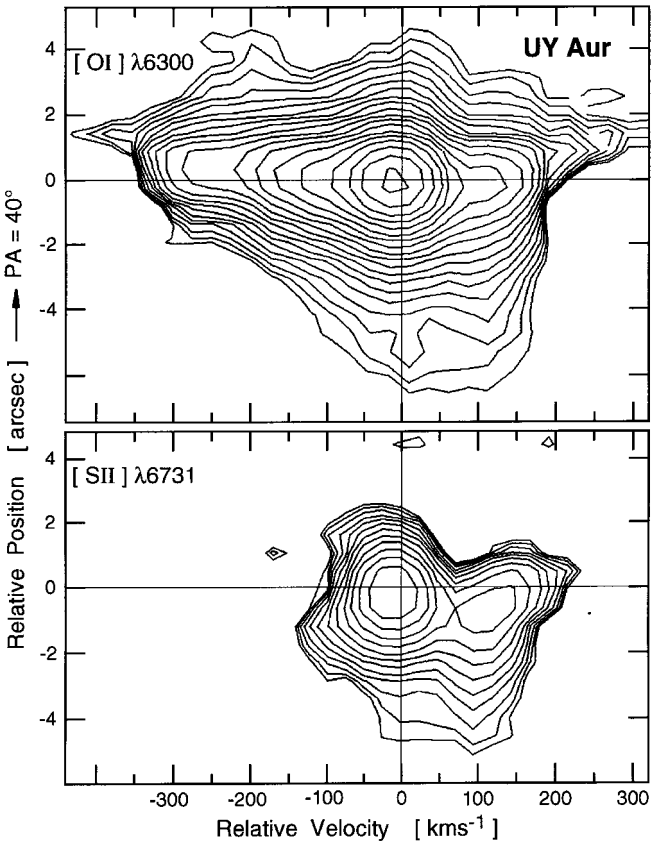

Fig. 15. Position-velocity maps of the [OI] λ6300 and [SII] λ6731 lines of UY Aur extracted from data taken with the 3.5 m Cassegrain twin spectrograph in December 1988 (PA = 40°). The stellar continuum has been subtracted. Contours, relative positions and velocities as in Fig. 1

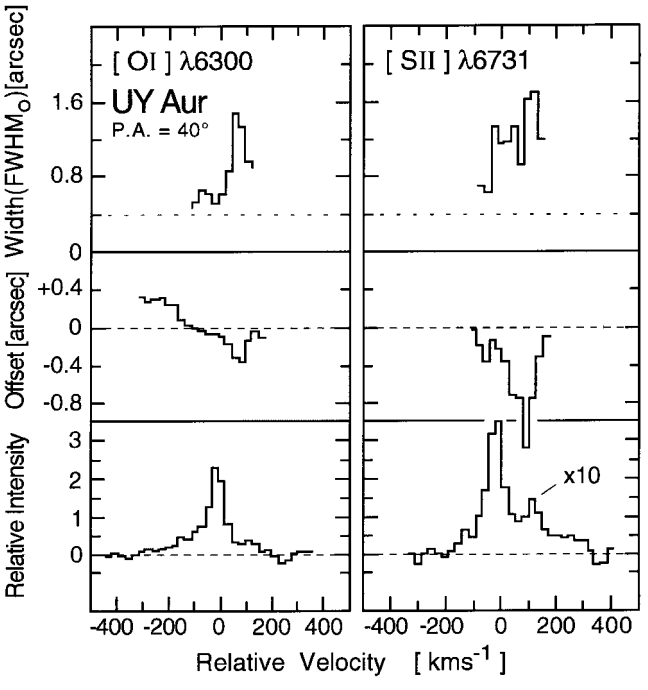

Fig. 16. Spatial width (top part), spatial offset (middle part) and spatially integrated intensity (lower part) of the [OI] λ6300 and [SII] λ6731 line emission of UY Aur as a function of the radial velocity (PA = 40°). The dotted line in the plots of the spatial width indicates the lower limit for which changes in width with velocity can be reliably measured. The radial velocity has been measured relative to the stellar velocity. The data are extracted from the continuum-subtracted position-velocity maps displayed in Fig. 15

(1994). These data clearly show both a blueshifted and a redshifted HVC and a slightly blueshifted LVC (see also below). The radial velocities of these two HVCs are -180 km s^{-1} and $+115$ km s^{-1}, respectively. Although one could have already concluded from the data of Hamann (1994) that RW Aur has a bipolar jet, the existence of such a jet has been first realized by Hirth et al. (1994b) from their long-slit spectroscopic observations. In their paper a preliminary discussion of some of the data shown here has been outlined.

A [SII] $\lambda\lambda$6716, 6731 image of the bipolar jet of RW Aur has been obtained by Mundt & Eislöffel (1997). From this image a PA of 130° and a projected length of 106″ have been derived for the southeastern blueshifted jet. On the opposite side the flow can be traced over at least 50″.

The five long-slit spectrograms of RW Aur (PA = 30°, 35°, 79°, 80° and 125°) have been taken before the above mentioned [SII] image. The analysis of these spectra resulted in a PA of 125° ± 15° for the blueshifted part of the bipolar outflow in good agreement with the imaging data. In the long-slit spectra the bipolar jet can be traced over a distance of 20″ only in each direction. This is not only due to the limited S/N ratio of the spectroscopic data but also due to the imperfect match of the PA of the slit with the outflow direction. From the variation of the offsets of the blue and redshifted emission centroids measured for different slit PA we conclude that RW Aur A is most probably the source of the bipolar outflow. This is particularly evident from the spectrogram obtained at PA = 79° (not shown here) for which the slit passes through component A and the closeby binary B&C. Although this spectrogram does not resolve the component A and the 2−3 mag fainter binary B&C the measured offsets of the HVC in the [SII] λ6731 line of only $\approx 0.2''$ from component A clearly show that the bipolar outflow must originate from RW Aur A. Note that unlike other TTSs with bipolar outflows, RW Aur shows no detectable reflection nebula on the continuum CCD frames obtained by Mundt & Eislöffel (1997).

A very surprising result of the data analysis of Hirth et al. (1994b) is the fact that the radial velocity of the HVC in the blue- and redshifted part of the outflow differs by about a factor of 2. This behaviour has been observed in several other TTSs as well but no satisfactory explanation for this unusual asymmetry between the two sides of the outflow has been found.

Further details on the variation of various spatial properties of the redshifted ($v \approx +100$ km s^{-1}) and blueshifted ($v \approx -175$ km s^{-1}) jet are shown in Fig. 17. From this figure it is evident that the two sides of the bipolar outflow differ not only in radial velocity but also in intensity, in N_e, and in the [SII]/[OI] line ratio. In addition, the Hα/[SII]$\lambda(6716+6731)$ line ratio differs between the two sides and values of that ratio ranging from 0.2 to 0.8 and from 1.0 to 3.3 have been measured for the redshifted and blueshifted jet, respectively. The direct images presented by Mundt & Eislöffel (1997) also show asymmetries between the redshifted and blueshifted jet in both the spatial extent and morphology.

Somewhat surprising and unusual is the fact that the N_e maximum of the redshifted part of the flow is not located at the stellar position but at a distance of $-0.9''$ from the star. The same behaviour is observed in the line intensity. On the other hand the [SII]/[OI] line ratio seems to be smallest at the stellar position as expected from observations of other TTSs.

As already discussed by Mundt et al. (1990) the decrease of the [SII]/[OI] line ratio with decreasing distance from the star probably results from a strong increase of N_e towards the star. As mentioned in that publication, this density effect only works near the critical density of the [SII] lines ($N_{e,\,crit.} \approx 10^4$ cm^{-3}) which is roughly 100 times lower than the critical density of the [OI] lines. Therefore, for $N_e > 10^4$ cm^{-3} the [OI] λ6300 line can still become stronger than the [SII] λ6731 line provided a low excitation is prevailing in the jet or the HH object. We note that the values of the [SII] λ6731/[OI] λ6300 ratio deduced for the more distant and therefore more tenuous parts of the redshifted outflow are typical for HH objects (1.5 ± 0.6; for more details see Dopita 1978; Brugel et al. 1981; Dopita et al. 1982).

In Fig. 18 the PV maps of the [OI] $\lambda\lambda$6300, 6363 and [SII] $\lambda\lambda$6716, 6731 lines are displayed. Further details on the spatial properties (spatial width and offset) in the [OI] λ6300 and [SII] λ6731 lines are shown in Fig. 19. Interestingly, a LVC is only observed in the [OI] lines but not in the [SII] lines. Similar results have been obtained only for DO Tau (see Sect. 3.5) and FN Tau (see Fig. 22a). We note that in the [OI] λ6363 line the LVC appears weaker relative to the [OI] λ6300 line (see Fig. 18). This presumably results from a blend with a weak (allowed) emission near 6300 Å (or is due to an underlying absorption feature near 6363 Å). As in most other TTSs discussed here the HVC shows a much larger spatial width and offset in the [SII] lines than in the [OI] lines.

3.9. V536 Aql

V536 Aql is a CTTS of spectral type K7 which is known for its relatively strong forbidden line emission in [OI] λ6300 ($W_\lambda = 13.9$ Å; Cohen & Kuhi 1979) and for its large degree of polarization ($P = 6.6\%$; Bastien 1982). Ageorges et al. (1994) have shown that V536 Aql is a double star. The components are separated by $0.52''$ in PA $= 17°$ and differ by about a factor of five in luminosity. Already Appenzeller et al. (1984) reported that the blueshifted [OI] λ6300 centroid is offset from the stellar position by about $1''$ in PA $= 90°$.

Long-slit spectra of the FELs of V536 Aql taken at various position angles (PA $= 20°$, $30°$, $60°$, $90°$, $110°$ and $157°$) suggest the existence of a bipolar outflow with the blueshifted part at a PA of $\approx 90° \pm 20°$. This outflow direction has been confirmed by recent narrow-band [SII] $\lambda\lambda$6716, 6731 images of V536 Aql by Mundt & Eislöffel (1997). These images show a few faint HH knots in PA $\approx 110°$ at a distance of about $10''$ to $15''$ from the star. We note that the outflow direction derived from our long-slit spectra could not be determined that accurately as for several other cases (e.g. like in the case of CW Tau; cf. Hirth et al. 1994a). This may be due to the large opening angle of the outflow of V536 Aql. It is also possible that light scattering of the emission from the FEL region in a compact reflection nebula is important, resulting in misleading offset values for the FELs. The latter is not unconceivable considering the large degree of polarisation of V536 Aql. Interestingly the outflow direction of PA $= 110°$ is not perpendicular to the position angle of the electric polarization vector of $65°$ (Bastien 1982), as observed for many outflows from YSOs (see e.g. Bastien 1989).

Because of the much larger luminosity of the component A we presume that this component is the outflow source. Figure 20 shows continuum-subtracted PV maps of V536 Aql in the [OI] λ6300, [NII] λ6583 and [SII] λ6731 lines taken in September 1993 at a PA of $90°$. The bipolar nature of this outflow is evident from the opposite spatial offsets of the blueshifted and redshifted emission. Interestingly the peak emission of the redshifted part of the outflow shows a radial velocity which is about 60% higher relative to V536 Aql compared to the blueshifted part. Similar asymmetries in the outflow velocities on either side of the bipolar outflow have been detected in several other TTSs (see e.g. Hirth et al. 1994b).

The spatial and kinematic properties of the [OI] λ6300, [NII] λ6583 and [SII] λ6731 lines derived from the corresponding PV maps are shown in more detail in Fig. 21. The intensity profiles show a double-peak in both the [OI] λ6300 and [SII] λ6731 lines. The centroid velocities for the HVC and LVC where determined to -77 km s^{-1} and -7 km s^{-1} for the [OI] λ6300 line and -91 km s^{-1} and $+1$ km s^{-1} for the [SII] λ6731 line, respectively. For the [NII] λ6583 line, as observed in all other investigated TTSs, only a HVC with a velocity of -71 km s^{-1} has been detected. In the [NII] λ6583 and in the [SII] λ6731 lines the redshifted part of the outflow can be traced up to $\approx +180$ km s^{-1}, which is not the case for the [OI] λ6300 line. Maybe the highly redshifted gas is relatively tenuous and of higher excitation and therefore not strongly emitting in [OI] λ6300 because of the higher critical density of the latter FEL.

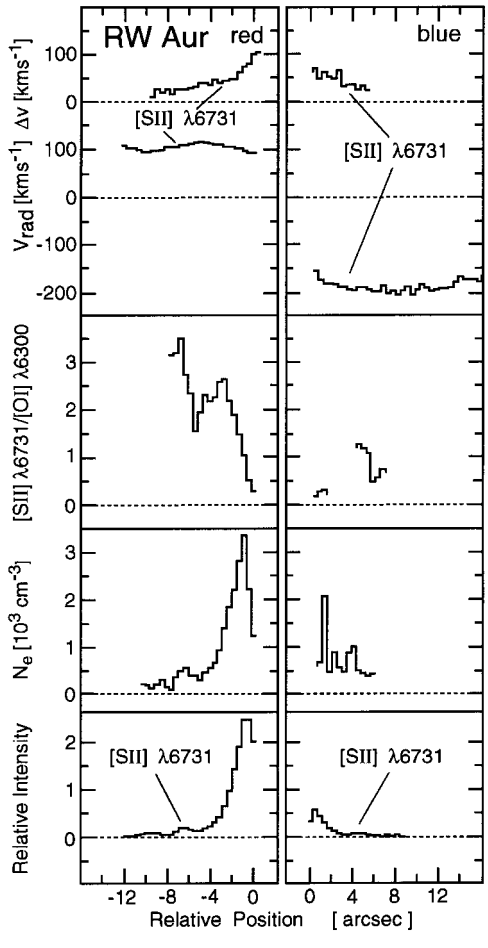

Fig. 17. Spatial variation of the velocity width (FWHM), the radial velocity of the [SII] λ6731 HVC, the [SII] λ6731/[OI] λ6300 line ratio, the electron density N_e, and the spatially integrated [SII] λ6731 intensity for the redshifted and blueshifted part of the bipolar outflow of RW Aur extracted from data taken with the 3.5 m Cassegrain twin spectrograph in November 1993 (PA = 125°). Positions and velocities as in Fig. 1. The velocity dispersion is corrected for the instrumental profile. The intensity is given in arbitrary units

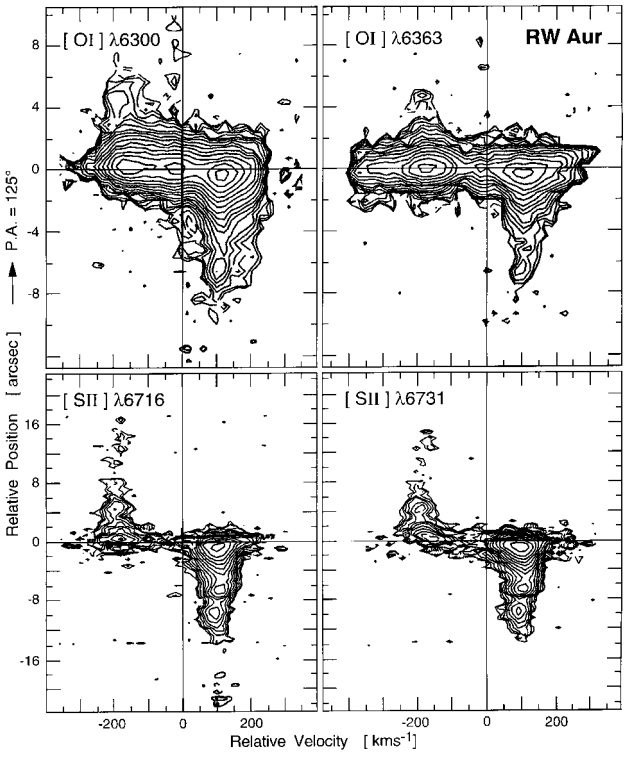

Fig. 18. Position-velocity maps of the [OI] λ6300, [OI] λ6363, [SII] λ6716 and [SII] λ6731 lines of RW Aur extracted from data taken with the 3.5 m Cassegrain twin spectrograph in November 1993 (PA = 125°). The stellar continuum has been subtracted. Contours, relative positions and velocities as in Fig. 1

Figure 21 shows that the offset value in all three FELs changes its sign at about the rest velocity of the star which clearly illustrates the bipolar nature of the outflow. In the blueshifted part of the outflow, the offset of the [SII] λ6731 HVC reaches values of up to 0.6″. For the blueshifted [NII] λ6583 HVC slightly higher offset values have been measured, whereas for the [OI] λ6300 HVC the offset is about half as large as in the other two FELs. As already mentioned above, this trend has been observed in most stars studied here (see Sect. 4.1 for more details).

The corresponding offsets for the LVC of the [OI] λ6300 and [SII] λ6731 lines are very small (0.1″ and 0.2″, respectively). The differences between the spatial properties of the HVC and the LVC are also illustrated in Fig. 21 where the offset and the spatial width as a function of the radial velocity are shown. In these plots a local minimum in the spatial width is observed in the radial velocity range of the LVC. As already mentioned above, similar results have been obtained for several other TTSs discussed here and elsewhere (Solf & Böhm 1993; Böhm & Solf 1994; Hirth et al. 1994a).

Finally, an offset value of 0.5″ of the [SII] λ6731 HVC has been deduced from our observations in September 1993. Comparing this value with the value of 0.7″ derived under similar observational conditions in September 1992 suggests that changes in the spatial structure of the outflow have occured within one year. However, further observations are required to prove the reality of this effect.

4. Main results of the survey and discussion

The main results of our long-slit spectroscopic survey of the FELs of TTSs are summarized in Table 2 and Fig. 22.

For each TTS studied Table 2 shows the spatial properties (offset and width) and kinematical properties (radial velocity and velocity dispersion) of the indiviual FELs on both sides of the outflow (if bipolar). Furthermore, if possible, the spatial and kinematic properties are listed separately for the LVC and HVC. However, in several cases it has not been possible to resolve spectroscopically these

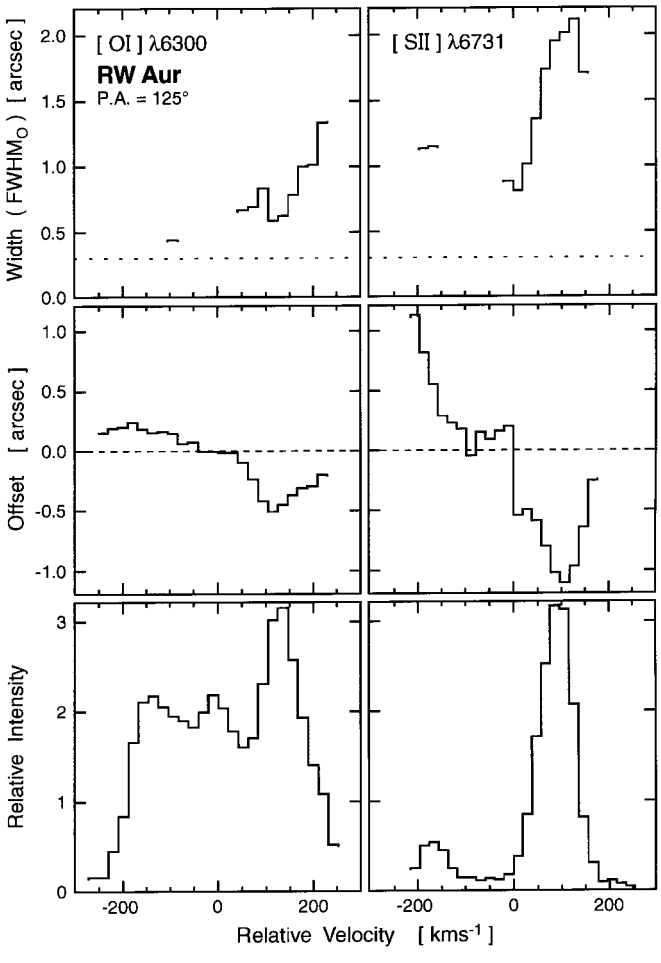

Fig. 19. Spatial width (top part), spatial offset (middle part) and spatially integrated intensity (lower part) of the [OI] λ6300 and [SII] λ6731 line emission of RW Aur as a function of the radial velocity (PA = 125°). The dotted line in the plots of the spatial width indicates the lower limit for which changes in width with velocity can be reliably measured. The radial velocity has been measured relative to the stellar velocity. The data are extracted from the continuum-subtracted position-velocity maps displayed in Fig. 18

two components mostly because their internal velocity dispersion is larger than their separation in radial velocity. Furthermore it is not clear in several cases whether we observe a LVC or a HVC. It will always be difficult to distinguish a LVC from a HVC resulting from a jet which is located close to the plane of the sky. In these cases we have printed all entries of Table 2 between the corresponding columns of the HVC and LVC (see also comments to individual objects). We note that the [NII] λ6583 line, if present, is regarded as a reliable indicator that a HVC indeed exists since all available [NII] intensity profiles suggest that this line probably never exhibits a LVC. In addition it is known from Hartigan et al. (1995) that many TTSs with small IR excesses ($K-L \leq 0.6$) probably have a LVC only. The objects printed in bold face in Table 2 are those for which the most detailed information is available and for which the outflow direction is known (from direct imaging and/or from long-slit spectroscopy) and which are closeby (usually at distances of 150 pc, except V536 Aql, which is at 200 pc). There are three more objects listed in Table 2 for which the outflow direction is known (FS Tau B, Bretz 4 and AS 353 A) but which are not printed in bold face, because either they are more distant and hence a derivation of their spatial properties makes little sense due to our limited spatial resolution or the central star is too faint to provide a reliable spatial reference for the determination of the offset and the spatial resolution (e.g. FS Tau B).

In Fig. 22 we show the profiles of the FEL profiles of all studied TTSs. In all cases, the data with the highest spectral resolution available are printed. These profiles are obtained by spatially integrating the data on the long-slit spectrograms. For comparison we also show the Hα line, which is in most cases much broader than the FELs and often shows a different line profile structure.

4.1. Spatial properties

Many of the TTSs in Table 2 show *spatially extended* FEL regions on a 1″ scale, especially in the HVC (see also below). This is one of our main results which was not expected a decade ago. Of the 38 TTSs listed in Table 2 we have derived information on the spatial properties of the FELs in 33 cases. A total of 27 TTSs of this sample show at least one FEL with an emission centroid which is spatialIy offset from the stellar position. In the [SII] λ6731 line the spatial offset of the high-velocity gas can reach values up to a few arcsec. Typical values are 0.3″ to 1.0″. For the spatial width the values range from the smallest measurable values ($\approx$ 0.3″; depending on the seeing and the S/N ratio) up to 2.9″. Typical values are 0.8″ to 1.5″.

In order to derive more detailed information on the spatial properties of the FELs it is important to compare the spatial properties of the different emission lines and the different properties between the high-velocity and low-velocity gas. We will perform that comparison mainly on the basis of those 12 TTSs studied in greatest detail (i.e. for those TTSs printed in bold face in Table 2). We will first compare the properties of their HVCs. If the existence of a well separated HVC is not clearly evident in the line profiles, e.g. if it is blended with a LVC, we will compare the spatial width and offset at velocities typical for the HVC (50−150 km s^{-1}) or if the [NII] λ6583 line is detected at the velocity of this line. (As already mentioned above, the [NII] λ6583 line never shows a LVC but only forms a HVC). Comparing the [OI] λ6300, [NII] λ6583 and the [SII] λ6731 lines it turns out that in general the spatial width and offset of the high-velocity gas is *largest* in [NII] and *smallest* in [OI]. In the following we will give more detailed information on this important result: In all 12 TTSs the measured offsets in [SII] are larger by a typical factor of 2 − 4 than in [OI]. However, the offsets in [NII]

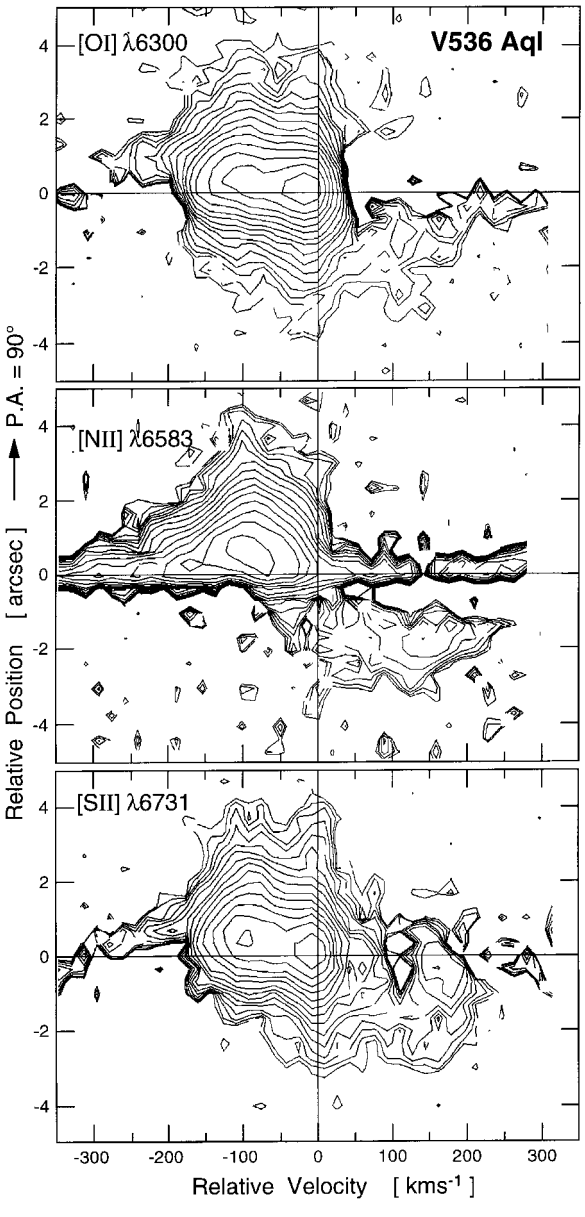

Fig. 20. Position-velocity maps of the [OI] λ6300, [NII] λ6583 and [SII] λ6731 lines of V536 Aql extracted from data taken with the 4.2 m ISIS Cassegrain spectrograph in September 1993 (PA = 90°). The stellar continuum has been subtracted. This subtraction could not be carried out perfectly for the [NII] λ6583 line due to the presence of the strong Hα line wing. Contours, relative positions and velocities as in Fig. 1

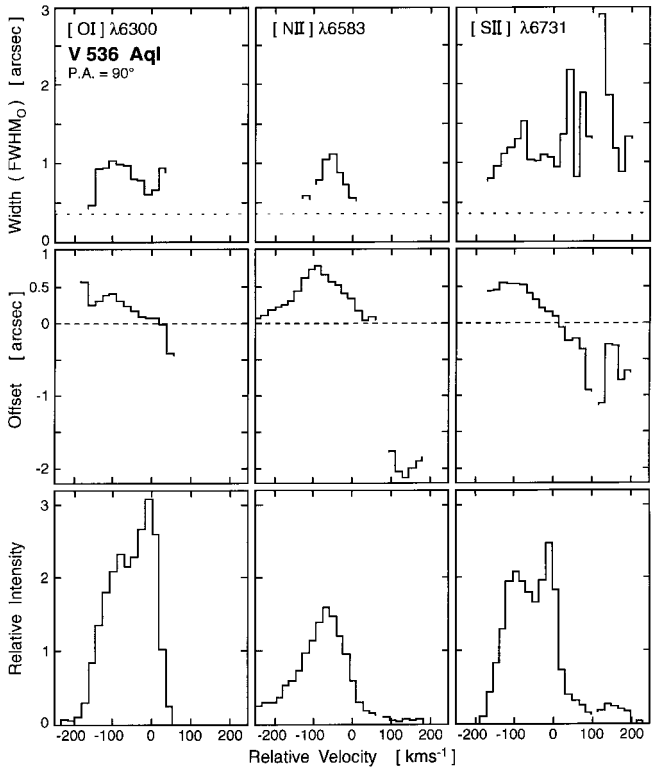

Fig. 21. Spatial width (top part), spatial offset (middle part) and spatially integrated intensity (lower part) of the [OI] λ6300, [NII] λ6583 and [SII] λ6731 line emission of V536 Aql as a function of the radial velocity (PA = 90°). The dotted line in the plots of the spatial width indicates the lower limit for which changes in width with velocity can be reliably measured. The radial velocity has been measured relative to the stellar velocity. The data are extracted from the continuum-subtracted position-velocity maps displayed in Fig. 20

are larger than in [SII]. From the 9 cases for which both [SII] and [NII] data are available (counting each side of a bipolar flow separately) 7 cases show offsets in [NII] clearly larger than those in [SII] by a typical factor of 1.5−2, while 2 cases show similar offsets.

With regard to the spatial widths it has been found also that the values are smallest in [OI] and largest in [NII] and [SII]. However, in [NII] and [SII] similar widths have been obtained in most cases. Due to the fact that the spatial width cannot be measured that accurately (see also Sect. 2) any small differences between [NII] and [SII] will not be detectable in our data. In 11 of the 13 cases with available data on the spatial width, the values in [SII] are larger by a factor of $1.5 - 3$ than those in [OI] and similar values have been obtained in the remaining 2 cases. From 10 cases where both [NII] and [SII] data are available similar values have been measured in 5 cases. In 3 cases the spatial width is larger in [NII] than in [SII] (by a factor of 1.3 to 2.0) and in 2 cases it is smaller than in [SII] (by a factor of 2). Note again that each side of a bipolar flow is counted as an individual case.

A comparison of the spatial properties of the HVC and LVC is more difficult since among the 12 most well studied TTSs only 3 stars (CW Tau, DG Tau and V536 Aql) show sufficiently separated HVCs and LVCs which can be individually studied with the medium resolution 3.5 m Cassegrain twin spectra. In order to include also the remaining 9 TTSs in our study we compare in these stars the spatial width and offset of the high-velocity gas (with radial velocities of $\pm 50 - 150$ km s^{-1}) with the

properties of the gas around the stellar velocity. For the sake of simplicity we will designate in the following comparison the emission from the gas at high and low velocity "HVC" and "LVC", respectively. Since in [NII] no LVC is observed this comparison is only useful for [OI] and [SII]. As expected from previous studies (e.g. Hirth et al. 1994a) in most cases the HVC shows a much larger offset and spatial width. In [OI] the offset of the HVC is significantly larger by a factor $2-3$ than that of the LVC in 8 out of the 10 cases with available data. Similar values of the offset have been obtained for the remaining 2 cases. In [SII] in all 9 cases with available data the offset in the HVC is larger than that in the LVC (typically by a factor of $2-4$).

Comparing the spatial properties of the LVC between the [OI] and [SII] lines, the same trend as for the HVC is observed. In all 11 cases with available data the offset in [SII] is larger than in [OI] by typically a factor of 2. The typical spatial offsets of LVCs are $0.2''$ in the [SII] λ6731 line. The spatial widths of the LVC are in [SII] also larger than in [OI] by a factor of about 2.

These results on the spatial properties of the HVC and LVC of the studied FELs are not surprising, since similar data have been obtained in previous detailed studies on CW Tau (Hirth et al. 1994a) and DG Tau (Solf & Böhm 1994). These authors show that the gas in the HVC and LVC can have quite different excitation conditions and also different spatial properties (see also Hamann 1994). However our much larger sample shows that these differences in the spatial properties of the HVC and LVC are a general property of TTSs and not just a peculiarity of a few individual objects. Like in the above mentioned studies of CW Tau and DG Tau, we interpret the HVC and LVC in the context of a model proposed by Kwan & Tademaru (1988, 1995). According to this model, the HVC forms in a well-collimated high-velocity jet ($v \approx 150-300$ km s^{-1}) while the LVC forms in a more compact region with intrinsically much smaller flow speeds which may result from a disk wind or a disk corona.

As shown more quantitatively by Hamann (1994) the gas in the LVC is generally of higher density and lower excitation than the gas in the HVC. This also explains why the [NII] $\lambda\lambda$6548, 6583 lines never form a LVC but only a HVC. Why the spatial offset of the HVC is largest in [NII] and smallest in [OI] can easily be explained if the density in the jets is decreasing and the excitation is increasing with increasing distance from the star. For a jet with diverging stream lines (e.g. with constant opening angle; see also below) a decreasing density with increasing distance is rather obvious, but why the electron temperature is increasing is unclear (i.e. it is unclear why the shock velocities increase with distance). Nevertheless if the jets from TTSs have such properties near the source (i.e. at distances of the order of 100 AU to several 100 AU), it is quite clear that the jets will appear most compact in [OI] which samples the densest gas due to its high critical density ($N_{\rm e,\ crit.} \approx 10^6$ cm^{-3}), while the jets will appear much larger in [SII] $\lambda\lambda$6716, 6731 since for these lines the critical density $N_{\rm e,\ crit.}$ is about 100 times smaller than in [OI]. Since the [NII] line samples gas of even lower densities and higher excitation the jets are expected to appear most extended in these lines.

We like to mention that the LVC of [SII] can be spatially resolved in many objects and has a small but significant offset (typically $0.2''$) from the source. This is also evident in a detailed study of DG Tau by Solf & Böhm (1994) and CW Tau by Hirth et al. (1994a) where the offset of the LVC is increasing with increasing blueshift of the low-velocity gas. All these results have certainly important implications for any detailed model of the FEL gas in TTSs.

The bipolar jets which give rise to spatially resolvable FEL regions for closeby TTSs ($d \approx 100-300$ pc) often display apparent lenghts of only $100-500$ AU. However, these lenghts probably do not represent the true physical lenghts of the jets (which in some of the "classical" outflow sources extend up to about 1 pc) but probably only the brightest region in which forbidden line emission can be detected (see below). It should be pointed out that previous studies have already shown that some spatially extended jets, like the ones from HH 30 or HL Tau (see Mundt et al. 1990), strongly decrease in their surface brightness with increasing distance from the source. Such a behaviour can be reasonably explained by the following considerations. Let us assume that the jet can be approximated by a homogenously filled cone at a given distance r from the star and $T_{\rm e} = $ const., say 10^4 K. Since $N_{\rm e} \propto r^{-2}$ holds for a cone of constant opening angle and since the emission measure per unit length of this cone is $\propto N_{\rm e}^2 r^2$ (for $N_{\rm e} < N_{\rm e,\ crit.}$) the brightness $I_j(r)$ of a spatially unresolved jet will be $I_j(r) \propto r^{-2}$. This means, that if $T_{\rm e}$ is constant and $N_{\rm e} < N_{\rm e,\ crit.}$ the brightness of a cone-like jet with a constant opening angle should strongly decrease with increasing distance from the source and therefore only the brightest regions will be detectable.

Interestingly, only 12 out of a sample of 27 TTSs with spatially extended FEL regions are known to be associated with a reflection nebula. This means that the TTSs in our sample have on average much fainter and smaller reflection nebulae than the "classical" outflow sources associated with HH objects and HH jets (cf. Mundt et al. 1987). In the latter sample, nearly all sources are associated with reflection nebulae detectable on the POSS or on continuum-light CCD images. These differences can probably be explained by evolutionary effects, with the classical HH object and jet sources representing a sample of on average younger stars than the CTTSs listed in Table 2 and therefore many of the HH jet sources are still associated with dense gas and dust from remnants of their parental molecular cloud.

Recent HST images of objects like HH 30 or HL Tau (Stapelfeldt et al. 1995; Ray et al. 1996; Burrows et al. 1996) have shown that YSOs can be associated with rather

compact reflection nebulae which appear stellar-like on ground-based images. If there are such bright reflection nebulae with sizes $< 1''$ around many CTTSs in our sample then scattering of the light from the FEL regions may affect significantly the determined spatial and kinematic properties in some cases (see also Noriega-Crespo et al. 1991). In HL Tau, for example, the LVC has a similar spatial width as the HVC ($1''$ at FWHM). In this case this result can probably be explained by the fact that one does not observe in the optical the star itself but rather its very compact reflection nebula only since the star itself is highly obscured by the circumstellar dust. Therefore the position derived from the continuum spectrum of the star will not be representative of the true stellar position. Light scattering may also explain why some [OI] λ6300 line profiles have a broad red wing as observed e.g. for CW Tau and several other CTTSs (Hirth et al. 1994a). This would be the case if the scattering dust would "see" the blueshifted jet as a receeding jet (i.e. if the scattering dust would be located between the star and that region producing most of the blueshifted forbidden line emission of the jet). We note that these broad red wings have been interpreted by Hirth et al. (1994a) in terms of rotation in the formation region of the LVC. The light scattering considered here is a reasonable alternative interpretation.

Several of our investigated sources are double stars (DD Tau, T Tau, XZ Tau, UY Aur and V536 Aql) separated by less than $1''$ (e.g. Leinert et al. 1993; Ghez et al. 1993, Ageorges et al. 1994). This appears to be an important result and suggests that also TTSs in double or multiple systems with small separations (≈ 100 AU) form jets. Since the subset of known binaries in that separation range is very small we have not investigated any possible correlation between the properties of the flow and the binary systems (e.g. between the position angle of the binary and the outflow direction). Certainly future HST observations would be helpful to answer various interesting questions (e.g. which of the two components of the binary is responsible for the jet, or do both components show individual outflows, or how well aligned are the outflows from both components).

4.2. Spectral properties

About 25% of the TTSs of our sample show only the [OI] $\lambda\lambda$6300, 6363 lines in the investigated wavelength range (6250 Å – 6750 Å) for a detection limit of ≈ 0.1 Å. In the [OI] λ6300 line a clearly recognizable double-peaked line profile has been observed in about 50% of the TTSs in our sample of 33 objects with high S/N [OI] λ6300 line profiles. For comparison, in the sample of Hartigan et al. (1995), which contains 32 stars and which is of similar or even higher spectral resolution, this fraction was about 43%. Note that our sample includes about half the objects of the sample of Hartigan et al. (1995) and that both samples have been more or less picked on a random basis. Whether the TTSs showing only a single velocity component in their [OI] lines have different physical conditions in their FEL regions is unclear. As already outlined above there are several reasons why both components could be blended into one component, even for a sufficiently large spectral resolution. For 3 stars in our sample (FN Tau, DO Tau and RW Aur) the LVC was only observed in the [OI] lines but not in the [SII] lines. The same is the case for a few stars in the sample of Hartigan et al. (1995) and Hamann (1994), namely CI Tau, DK Tau, DL Tau, HM Lup, AS 353 A and SCrA. Since in all these stars the HVC is detected in both the [OI] lines and [SII] lines a much higher density (and/or lower excitation) is indicated for the LVC as compared to the HVC, at least in these stars, but probably in a large fraction of the TTSs (see Hartigan et al. 1995).

For 40% of the investigated objects we have detected the [NII] λ6583 line. In the sample of Hartigan et al. (1995) this fraction was 37%. Apparently this fraction does not depend much on the detection limit since the detection limit of Hartigan et al. (1995) for FELs has been about 3 times higher than in our study.

Table 2. (See following pages) Spatial and kinematical properties of the FEL regions of the studied TTSs. In the case of known bipolar outflows, the values are quoted separately for the blueshifted and redshifted part of the outflow. The kinematical data listed are derived from the spectra with the *highest* spectral resolution available (see also Fig. 22). Uncertain values are quoted in parentheses. Note that in several cases it has not been possible to resolve the two velocity components or it is not clear whether the data represent a LVC or a HVC with small radial velocities. In these cases all entries are inserted in Table 2 between the corresponding columns of the HVC and LVC (see also comments to individual objects). Columns: (1) Object number in survey. (2) Number in the Herbig & Bell (1988) catalogue. (3) Name of the object; printed in bold face for closeby ($d \leq 200$ pc) and most well studied objects with known outflow direction. (4) Number of campaign (see Table 1). (5) Investigated FEL. (6) Position angle (PA) of the outflow derived either from direct imaging or long-slit spectroscopy. (7) PA of the long-slit spectrogram from which the quoted spatial data have been derived. The PA is given for the blueshifted forbidden line emission. (8) and (9) Radial velocity of the HVC and LVC relative to the stellar velocity. (Asterisks denote heliocentric velocities). (10) and (11) Velocity dispersion (FWHM) of the HVC and LVC corrected for the instrumental profile. (12) and (13) Spatial offset of the emission centroid of the HVC and LVC relative to the stellar position. (14) and (15) Spatial width ($FWHM_0$) of the HVC and LVC corrected for the spatial resolution (see Sect. 2). (16) and (17) Equivalent width of the HVC and LVC derived from Gaussian fitting to these two components. (18) Total equivalent width. Note that is some cases this value is not always the sum of the individual values of the HVC and LVC due to the non Gaussian profile of these components. (19) An asterisk indicates that remarks on the TTS are available

Table 2.

(1) #	(2) HBC #	(3) Object	(4) Camp. #	(5) Line	(6) PA flow [deg]	(7) PA slit [deg]	(8) v_{HVC} [kms^{-1}]	(9) v_{LVC} [kms^{-1}]	(10) Δv_{HVC} [kms^{-1}]	(11) Δv_{LVC} [kms^{-1}]	(12) offset y HVC [arcsec]	(13) offset y LVC [arcsec]	(14) width Δy_0 HVC [arcsec]	(15) width Δy_0 LVC [arcsec]	(16) Wλ HVC [Å]	(17) Wλ LVC [Å]	(18) Wλ total [Å]	(19) Rem.
1	23	FM Tau	7	[OI] λ6300		90	−1		65		(0.0)						−0.6	*
2	24	FN Tau	7	[OI] λ6300		90	−117	−26	67	80					−0.7	−0.4	−1.3	*
			7	[SII] λ6731		90	−120	(−25)	76	(123)					−0.4	−0.1	−0.5	
3	25	CW Tau	3	[OI] λ6300	144	160	−104	+2	83	39	−0.3	−0.1	1.0	<0.5	−1.6	−1.8	−3.5	*
			3	[NII] λ6583	144	160	−109		57						−0.3		−0.3	
			3	[SII] λ6731	144	160	−95	−12	66	5	−1.0	−0.2	1.8	1.0	−0.9	−0.4	−1.4	
			3	[SII] λ6731	324	160	+112											
4	30	DD Tau		[SII] λ6731	≈90	94	−73				−0.6							*
				[SII] λ6731	≈270	94	+79				+0.8							
5	31	CZ Tau	9	[OI] λ6300		11	+15		≈130							(−1.6)		*
6	34	RY Tau	3	[OI] λ6300		60	−79	−4	70	39	0.0	0.0	0.7	<0.5	−0.3	−0.3	−0.6	*
			3	[SII] λ6731		0	(−113)	(−28)	(60)	(109)							−0.2	
7	381	FS Tau B	2	[OI] λ6300	54	56	−38		177								−4.3	*
			2	[NII] λ6583	54	56	−54		97								−2.0	
			2	[NII] λ6583	234	56	+42		<20									
			2	[SII] λ6731	54	56	(−63)		(124)								−1.0	
			2	[SII] λ6731	234	56	+44		37									
8	383	FS Tau A	4	[OI] λ6300		328	−5		49		−0.3		<0.5				−12.7	*
			4	[NII] λ6583		328	−5		50		0.0		<0.5				−5.6	
			4	[SII] λ6731		328	−1		38		−0.1		<0.5				−6.3	
9	35	T Tau		[OI] λ6300	≈270	270	−111	−5	90	46	−0.1	(−0.3)	0.7	(1.3)				*
				[SII] λ6731	≈270	270	−121	−5	65	27	−0.3	(−0.6)	1.2	(1.7)			−1.0	
10	36	DF Tau	3	[OI] λ6300		19	−84	−5	69	44	+0.2	+0.2	<0.5	<0.5	−1.1	−0.9	−2.0	
			4	[NII] λ6583		212	−84		60						−0.1		−0.1	
11	37	DG Tau		[OI] λ6300	226	226	−250	−43		65	+0.7	+0.1	0.3	0.3				*
				[NII] λ6583	226	226	−210				+1.5						−0.8	
				[SII] λ6731	226	226	−210	−43		39	+2.2	+0.2		0.3			−2.1	
12	389	Haro 6-10	9	[OI] λ6300	≈240	247	−37		104		−0.1		0.9				−3.8	*
			2	[NII] λ6583	≈240	247	−79		90		−0.6		1.9				−1.0	
			2	[SII] λ6731	≈240	247	−47		88		−0.3		1.7				−2.4	
13	38	DH Tau	7	[OI] λ6300		90	−4		58		+0.2		<0.4				−1.0	*
14	45	DK Tau	7	[OI] λ6300		90	−82	−6	81	62	0.0	+0.1	<0.4	0.8			−0.8	

Table 2. continued

(1) #	(2) HBC #	(3) Object	(4) Camp. #	(5) Line	(6) PA flow [deg]	(7) PA slit [deg]	(8) v_{HVC} [kms^{-1}]	(9) v_{LVC} [kms^{-1}]	(10) Δv_{HVC} [kms^{-1}]	(11) Δv_{LVC} [kms^{-1}]	(12) offset y HVC [arcsec]	(13) LVC [arcsec]	(14) width Δy_0 HVC [arcsec]	(15) LVC [arcsec]	(16) Wλ HVC [Å]	(17) LVC [Å]	(18) Wλ total [Å]	(19) Rem.
15	49	HL Tau	5	[OI] λ6300	51	50	−201	−19	40	52	+0.4	+0.1	1.9	<0.7	−3.3	−0.7	−4.0	*
			5	[NII] λ6583	51	50	−215		44		+0.4		0.8		−1.5		−1.5	
			5	[SII] λ6731	51	50	−210	−9	41	32	+0.6	+0.4	1.5		−1.9	−0.5	−2.8	
16	50	XZ Tau	4,5	[OI] λ6300	15	19	−54	+4	133	13	+0.2		1.0				−12.1	*
			4,5	[OI] λ6300	195	19	≈+125				−0.2		1.8					
			4,5	[NII] λ6583	15	19	−69		74		+1.4		3.4				−1.7	
			4,5	[NII] λ6583	195	19	≈+125				−0.4		0.9					
			4,5	[SII] λ6731	15	19	−70	−7	78	11	+1.3		2.9				−4.0	
			4,5	[SII] λ6731	195	19	≈+125				−0.3		1.8					
17	52	UZ Tau E	2,4	[OI] λ6300	≈20	0	−107	−10	57	96	+0.1		<0.3				−7.8	*
			2,4	[OI] λ6300	≈200	0	≈+90				−0.1		0.5					
			2,4	[NII] λ6583	≈20	0	−86		101		+0.3		0.7				−0.5	
			2,4	[NII] λ6583	≈20	0	≈+90				−0.4		<0.3				−0.5	
			2,4	[SII] λ6731	≈20	0	−103	−11	85	67	+0.2		0.4				−0.9	
			2,4	[SII] λ6731	≈200	0	≈+90				−0.1		0.6					
18	55	GH Tau	7	[OI] λ6300		90	(−63)	−4	(110)	58	−0.5	−0.1	<0.4	<0.4	−0.3	−0.6	−0.8	*
19	58	DL Tau	9	[OI] λ6300		11	−145	−7	97	98	−0.1	0.0	1.6	0.8	−0.3	−0.3	−0.7	
			9	[SII] λ6731		11	−145		132						−0.3		−0.3	3
20	60	HN Tau	5,9	[OI] λ6300	≈350	0	(−56)	(−16)	(124)	(49)	−0.1		<0.4				−13.6	*
			5	[NII] λ6583	≈350	0	−84		104		−0.4		0.7		−1.1		−1.1	
			5	[SII] λ6731	≈350	0	(−66)	(−19)	(123)	(18)	−0.2		0.9		−1.7	−1.3	−3.0	
21	63	AA Tau	9	[OI] λ6300		11		−7		104		(−0.1)					−1.1	*
			9	[NII] λ6583		11	−33		59		−0.5		1.3				−0.2	
22	67	DO Tau	3	[OI] λ6300	250	250	−85	−17	38	73	0.0	0.0	<0.4	<0.4	−2.9	−1.3	−4.2	*
			3	[OI] λ6300	70	250	+202											
			3	[SII] λ6731	250	250	−98		21		+0.4		1.2		−0.9		−1.1	
			3	[SII] λ6731	70	250	+211											
23	70	DP Tau	7	[OI] λ6300	221	222	≈−100	−2			−0.1	0.0	0.4	< 0.3	−0.7		−0.7	*
			7	[NII] λ6583	221	222	−64				−0.7		1.4		−0.2		−0.2	
			7	[NII] λ6583	41	222	+29	2	86		+0.4		0.7		−0.6		−0.6	
			7	[SII] λ6716	41	222	+25		85		+0.2		0.8		−2.1		−2.1	
24	72	DQ Tau	9	[OI] λ6300		42		−27		90		0.0		<0.4			−2.8	*
			9	[SII] λ6731		42		−19		66		0.0		<0.4			−0.2	
25	74	DR Tau	3	[OI] λ6300	(93)	93	−153	+2	30	27	+0.1	+0.1	<0.5	<0.5	−0.4	−0.3	−0.7	*
			3	[SII] λ6731	(93)	93	−149		22						−0.1		−0.1	

Table 2. continued

(1) #	(2) HBC #	(3) Object	(4) Camp. #	(5) Line	(6) PA flow [deg]	(7) PA slit [deg]	(8) v_{HVC} [kms^{-1}]	(9) v_{LVC} [kms^{-1}]	(10) Δv_{HVC} [kms^{-1}]	(11) Δv_{LVC} [kms^{-1}]	(12) offset y HVC [arcsec]	(13) offset y LVC [arcsec]	(14) width Δy_0 HVC [arcsec]	(15) width Δy_0 LVC [arcsec]	(16) Wλ HVC [Å]	(17) Wλ LVC [Å]	(18) Wλ total [Å]	(19) Rem.
26	76	UY Aur	5	[OI] λ6300	≈40	40	≈-100	-8		25	(+0.2)	-0.1		0.6		-0.7	-0.7	*
			5	[SII] λ6731	≈40	40		-13		46		-0.2		1.2		-0.2	-0.2	
			5	[SII] λ6731	≈120	40	(+60)				-0.9		1.4					
27	80	RW Aur	9	[OI] λ6300	130	125	-167	-8	129	106	+0.2	0.0	<0.3	<0.3	-0.7	-0.1	-0.8	*
			9	[OI] λ6300	310	125	122				-0.5		0.6					
			9	[SII] λ6731	130	125	-163		99		+0.6		1.1					
			9	[SII] λ6731	310	125	99				-1.1		2.0					
28	98	HS Ori	4	[OI] λ6300		350	-59*		149								-8.3	*
29	106	VZ Ori	9	[OI] λ6300		340	-23		46		-0.2		0.0				-0.7	*
30	161	PU Ori	4	[OI] λ6300		350	-152	-27	49	144	0.0	+0.1	0.7	<0.5	-0.4	-0.8	-1.2	*
31	177	V510 Ori	9	[OI] λ6300		340	-45		108		0.0				-4.1		-4.1	*
			9	[NII] λ6583		340	-11		51		-0.1				-0.7		-0.7	
			9	[SII] λ6731		340	-69		88		0.0				-0.9		-0.9	
32	507	LkHα 313	4	[OI] λ6300		350	≈+45		≈180		+0.4		<0.6				-6.7	*
33	198	Bretz 4	9	[OI] λ6300	343	343	≈-170	-21	250	65	-0.1	0.0	0.8	.8	-1.1	-1.4	-2.5	*
34	523	V481 Mon	4	[OI] λ6300		350	+29*		101		0.0		<0.5				(-3.5)	*
35	216	NX Mon	4	[OI] λ6300		350	≈+50		≈400		0.0		<0.5				(-4.4)	*
36	292	AS 353 A	3	[OI] λ6300	109	107	-270	-9	≈100	≈80	+0.1	0.0	<0.4	<0.4	-0.5	-0.4	-1.3	*
				[OI] λ6300	289	107	+215		≈80			0.0		<0.4	-0.4			
37	294	V536 Aql	3	[OI] λ6300	110	90	-77	-7	132	18	+0.3	+0.1	1.1	0.7	-2.5	-1.8	-4.0	*
			3	[NII] λ6583	110	90	-71		93		+0.6		1.1				-1.2	
			3	[NII] λ6583	290	90	+160				-2.0							
			3	[SII] λ6731	110	90	-91	+1	65	27	+0.5	+0.2	1.2	1.0	-0.8	-0.6	-1.4	
			3	[SII] λ6731	290	90	≈+160				(-0.5)		(1.6)					
38	326	MacC sH15	9	[OI] λ6300		45	(-72)		(52)						-0.1		-0.1	*

Remarks to Table 2

FM Tau: Only a single velocity component with $v_{\rm rad} = -1$ km s^{-1} is visible. It is unclear whether this low-velocity emission results from a true LVC or is emission from a high-velocity jet seen edge-on (see also Fig. 22a).

FN Tau: The LVC in the [SII] lines is only marginally indicated (see also Fig. 22a).

CW Tau: All values are taken from Hirth et al. (1994a) where this object is discussed in detail. The counterjet in PA = 324° displays radial velocities between +50 und +180 km s^{-1}.

DD Tau: The values given in Table 2 are from Neckel & Staude (1993). In the [OI] λ6300 line profile (see Fig. 22b) the two components of the bipolar outflow are not resolved but apparently only the blueshifted side of the bipolar outflow has been detected in the [SII] λ6731 and [NII] λ6583 lines.

CZ Tau: The low S/N ratio of the obtained spectrogram does not allow detailed kinematical and spatial studies. The possible presence of a blueshifted and redshifted emission component in the [OI] λ6300 line profile (see Fig. 22b) has to be confirmed by deeper spectra.

RY Tau: The LVC is visible only in [OI] λ6300 (see Fig. 22c). The two possible components listed in Table 2 for the [SII] λ6731 line are derived from a two-component Gaussian fit to the profile.

FS Tau B: The kinematic data are based on a long-slit spectrogram published by Eislöffel & Mundt (1997).

FS Tau A: Only a single velocity component with $v_{\rm rad} = -5$ km s^{-1} has been detected (see also Fig. 22d). It is unclear whether this low-velocity emission results from a true LVC or if it originates from a high-velocity jet seen edge-on. However, the detection of [NII] λ6583 emission strongly argues in favour of the presence of a HVC, since we are not aware of any star where a true LVC also shows [NII] emission. Recent studies of Eislöffel & Mundt (1997) of the FS Tau A & B regions show that within a few arcsec from FS Tau A and at the position of FS Tau A there is extended HH emission. This emission probably results from a poorly collimated wind from FS Tau B when this wind hits the edges of a cavity. It is conceivable that at least part of the observed emission in FS Tau A is actually resulting from that extended HH emission. This would also explain the rather small line widths observed in the FELs of FS Tau A.

T Tau: All values are taken from Böhm & Solf (1994), where this rather complex object is discussed in detail.

DG Tau: All values are taken from Solf & Böhm (1993), where this object is discussed in detail.

Haro 6-10: This object is discussed in detail in the text; see Sect. 3.1.

DH Tau: Only a single velocity component with $v_{\rm rad} = -4$ km s^{-1} is visible (see also Fig. 22e). It is unclear whether this low-velocity emission results from a true LVC or if it is emission from a high-velocity jet seen edge-on. The small offset of the [OI] λ6300 emission of +0.2″ argues more in favour of a HVC.

HL Tau: This object has been studied in detail by Mundt et al. (1990). From HST observations of Stapelfeldt et al. (1995) and Ray et al. (1996) it is known that the star itself is not directly observable in the optical, but only its bright compact reflection nebula. Since all measured spatial quantities refer to the centroid of the registered continuum emission of the reflection nebula, the quoted offset values do not represent the offset with respect to the stellar position. Also the values for the spatial width are probably altered due to the presence of the reflection nebula.

XZ Tau: This object is discussed in detail in the text; see Sect. 3.2.

UZ Tau E: This object is discussed in detail in the text; see Sect. 3.3.

GH Tau : A broad emission line wing extending up to -200 km s^{-1} has been detected in the [OI] λ6300 line (see Fig. 22g). The value of -63 km s^{-1} for the radial velocity of the HVC is derived from a Gaussian fit to this broad blueshifted emission.

HN Tau: In none of the FEL profiles of this star are two components directly evident, but as discussed in the text (see Sect. 3.4) there are indirect arguments for the presence of both a LVC and a HVC derived from the observed [NII] line profile. The listed radial velocities and velocity dispersions for the HVC and LVC of the [OI] and [SII] lines are the result of a two-component Gaussian fit to the profiles of these two lines (see also Fig. 22h).

AA Tau: Only a single velocity component with $v_{\rm rad} = -7$ km s^{-1} is visible. It is unclear whether this low-velocity emission results from a true LVC or originates from a high-velocity jet seen edge-on. However, the presence of [NII] λ6583 emission at $v_{\rm rad} = -33$ km s^{-1} strongly argues that at least part of the [OI] λ6300 emission results from a HVC, since we are not aware of any star where a pure LVC also shows [NII] emission (see also Fig. 22i).

DO Tau: This object is discussed in detail in the text; see Sect. 3.5.

DP Tau: This object is discussed in detail in the text; see Sect. 3.6.

DQ Tau: It is unclear, whether the observed emission component seen in [OI] λ6300 and [SII] λ6731 at about -20 km s^{-1} is a LVC or is a HVC of a jet seen nearly edge-on (see also Fig. 22j).

DR Tau: The values for the spatial offset are near the detection limit. This is also the reason why it is hard to determine the outflow direction from the obtained long-slit spectrogram. Probably the outflow direction is towards the direction of the HH object found by Mundt & Eislöffel (1997) along PA = 93°. There might be another emission component between the HVC

and the LVC of the [OI] λ6300 line at $v_{\rm rad} \approx -80$ km s^{-1} (see also Fig. 22k).

UY Aur: This object is discussed in detail in the text; see Sect. 3.7.

RW Aur: This object is discussed in detail in the text; see Sect. 3.8.

HS Ori: Due to the relatively high radial velocity of the [OI] λ6300 line of $v_{\rm hel} = -59$ km s^{-1}, we believe that most of the emission originates in a HVC (see also Fig. 22l).

VZ Ori: Only a single velocity component with $v_{\rm rad} = -23$ km s^{-1} is visible (see also Fig. 22l). It is unclear whether this low-velocity emission results from a true LVC or if the emission originates from a high-velocity jet seen edge-on. However, the large $K - L$ value of 1.66 (Cohen & Kuhi 1979) favours more the interpretation of a HVC (for detailed arguments see Fig. 11 of Hartigan et al. 1995).

PU Ori: A very weak [SII] λ6731 emission at ≈ -50 km s^{-1} might be present ($W_\lambda \approx -0.2$ Å; see also Fig. 22m).

V510 Ori: Although only a single velocity component at relatively small radial velocities is visible in [OI] λ6300 ($v_{\rm rad} = -45$ km s^{-1}) and [SII] ($v_{\rm rad} = -69$ km s^{-1}), we believe that a significant portion of this emission results from a HVC (i.e. from a jet being nearly oriented in the plane of the sky). The main arguments for that interpretation are the presence of [NII] emission and the large line width (see also Fig. 22m).

LkHα 313: A very broad [OI] λ6300 emission (FWHM $\approx$ 180 km s^{-1}) is observed for this object. The emission peaks at $v_{\rm rad} = +45$ km s^{-1} (see also Fig. 22n). Maybe we observe, like for DD Tau a bipolar outflow whose two sides are not spectroscopically resolvable due to large internal line widths.

Bretz 4: This object is the source of a HH jet (HH 271-273) and has been first imaged in the [SII] $\lambda\lambda$6716, 6731 lines by Carballo & Eiroa (1992). The [OI] λ6300 line profile shows a LVC centered at $v_{\rm rad} \approx -20$ km s^{-1} and a very broad blueshifted wing of high-velocity emission extending to nearly -350 km s^{-1} (see also Fig. 22n). This high-velocity emission is approximately centered at $v_{\rm rad} \approx -170$ km s^{-1} ($\Delta v \approx -250$ km s^{-1}).

V481 Mon: Due to the faintness of the star, the S/N ratio of the data obtained is very low. Only a single velocity component with $v_{\rm hel} = +29$ km s^{-1} is visible (see also Fig. 22n). It is unclear whether the observed low-velocity emission results from a true LVC or if it originates from a high-velocity jet seen edge-on.

NX Mon: A very broad [OI] λ6300 emission (FWHM $\approx$ 400 km s^{-1}) is observed for this object (see also Fig. 22o). The emission peaks at $v_{\rm rad} \approx +50$ km s^{-1}. Maybe we observe, like for DD Tau, a bipolar outflow whose two sides are not spectroscopically resolvable due to large internal line widths.

AS 353 A: The extended bipolar outflow from this TTS traced by HH objects (HH 32 A-D) has been discussed in detail by Mundt et al. (1983), Hartigan et al. (1986), Solf et al. (1986) and recently by Davis et al. (1996). A [OI] λ6300 line profile of the star has been published by Hartigan et al. (1995). In addition to a slightly blueshifted LVC at -9 km s^{-1} a broad blueshifted high-velocity emission is observed, which extends up to -320 km s^{-1} (see Fig. 22o). For the intermediate velocities at -180 km s^{-1} the emission centroid is shifted $+0.3''$ relative to the source and the spatial width is about $1''$. For the [SII]-lines no spectra have been secured because these lines are extremely weak (W_λ of [SII] λ6716 equals 0.08 Å, Hartigan et al. 1995).

V536 Aql: This object is discussed in detail in the text; see Sect. 3.9.

MacC sH15: The emission in [OI] λ6300 is only barely detectable ($W_\lambda \approx 0.1$ Å) and the listed kinematical data are relatively uncertain (see also Fig. 22p).

Acknowledgements. We are indepted to the staff of the Calar Alto Observatory and the William Herschel Telescope for assistance during the various observing runs.

References

Ageorges N., Ménard F., Monin J.-L., Eckart A., 1994, A&A 283, L5
Appenzeller I., Jankovics I., Östreicher R., 1984, A&A 141, 108
Appenzeller I., Mundt R., 1989, A&AR 1, 291
Bastien P., 1982, A&AS 48, 153
Bastien P., 1985, ApJS 59, 227
Bastien P., 1989, in: Polarized Radiation of Circumstellar Origin, Coyne G.V. et al. (eds.). Vatican City, Vatican Obs., p. 541
Böhm K.-H., Solf J., 1994, ApJ 430, 277
Brugel E., Böhm K.-H., Mannery E., 1981, ApJS 47, 117
Burrows C.J., et al., 1996, ApJ 473, 437
Carballo R., Eiroa C., 1992, A&A 262, 295
Cohen M., Kuhi L.V., 1979, ApJS 41, 743
Davis C.J., Eislöffel J., Smith M.D., 1996, ApJ 463, 246
Dopita M., 1978, ApJS 37, 117
Dopita M., Binette L., Schwartz R.D., 1982, ApJ 261, 183
Edwards S., Cabrit S., Strom S.E., Heyer I., Strom K.M., Anderson E., 1987, ApJ 321, 473
Edwards S., Ray T.P., Mundt R., 1993, in Protostars and Planets III, Levy E.H. and Lunine J.I. (eds.). University of Arizona Press, p. 567
Eislöffel J., Mundt R., 1997 (in preparation)
Elias J.H., 1978, ApJ 224, 857
Ghez A.M., Neugebauer G., Matthews K., 1993, AJ 106, 2005
Gómez de Castro A.I., Pudritz R.E., 1993, ApJ 409, 748
Hamann F., 1994, ApJS 93, 485
Hartigan P., Mundt R., Stocke J., 1986, AJ 91, 1357
Hartigan P., Edwards S., Ghandour L., 1995, ApJ 452, 736
Hartmann L.W., Raymond J.C., 1989, ApJ 337, 903
Herbig G.H., 1977, ApJ 214, 747
Herbig G.H., Bell K.R., 1988, Third Catalog of Emission-Line Stars of the Orion Population, Lick Obs. Bull. 1111
Hirth G.A., Mundt R., Solf J., 1994a, A&A 285, 929
Hirth G.A., Mundt R., Solf J., Ray T.P., 1994b, ApJ 427, L99
Jankovics S., Appenzeller I., Krautter J., 1983, PASP 95, 883
Jensen E.L.N., Koerner D.W., Mathieu R.D., 1996, AJ 111, 2431
Kwan J., Tademaru E., 1988, ApJ 332, L41
Kwan J., Tademaru E., 1995, ApJ 454, 382
Leinert Ch., Haas M., 1989, ApJ 342, L39

Leinert Ch., Zinnecker H., Weitzel N., Christou J., Ridgway S.T., Jameson R., Haas M., Lenzen R., 1993, A&A 278, 129
Mundt R., Hirth G.A., 1997 (in preparation)
Mundt R., Eislöffel J., 1997 (in preparation)
Mundt R., Brugel E.W., Bührke T., 1987, ApJ 319, 275
Mundt R., Stocke J., Stockman H.S., 1983, ApJ 265, L71
Mundt R., Ray T.P., Bührke T., 1988, ApJ 333, L69
Mundt R., Ray T.P., Bührke T., Raga A.C., Solf J., 1990, A&A 232, 37
Mundt R., Ray T.P., Raga A.C., 1991, A&A 252, 740
Neckel T., Staude H.-J., 1993, in Mitt. Astron. Ges. 76, 279
Noriega-Crespo A., Calvet N., Böhm K.-H., 1991, ApJ 379, 676
Ouyed R., Pudritz R.E., 1993, ApJ 419, 255
Ouyed R., Pudritz R.E., 1994, ApJ 423, 753
Ray T.P., Mundt R., Dyson J.E., Falle S.A., Raga A.C., 1996, ApJ 468, L103
Reipurth B., 1994, A general catalogue of Herbig-Haro objects, electronic publication, available through anonymous ftp from ftp.hq.eso.org in /pub/Catalogs/Herbig-Haro
Solf J., 1989, in: ESO Conf. Proc. 33, Low Mass Star Formation and Pre-Main Sequence Objects, Reipurth B. (ed.). Garching b. München, p. 399
Solf J., Böhm K.-H., 1993, ApJ 410, L31
Solf J., Böhm K.-H., Raga A.C., 1986, ApJ 305, 795
Stapelfeldt K.R., et al., 1995, ApJ 449, 888
Strom K.M., Strom S.E., Wolff S.C., Morgan J., Wenz M., 1986, ApJS 62, 39

Fig. 22. Line profiles of the [OI] λ6300, [NII] λ6583, [SII] λ6731 lines and the Hα line of all TTSs from our survey extracted from spectrograms taken with the 2.2 m coudé spectrograph (c), the 3.5 m Cassegrain twin spectrograph (T) and the 4.2 m ISIS Cassegrain spectrograph (I). The radial velocities (in km s^{-1}) are relative to the stellar velocity except for HS Ori, LkHα 313 and V481 Mon. For these three stars heliocentric velocities are given. For all FEL profiles the continuum has been subtraced. For both the Hα and FEL profiles the line intensity is normalized to the continuum

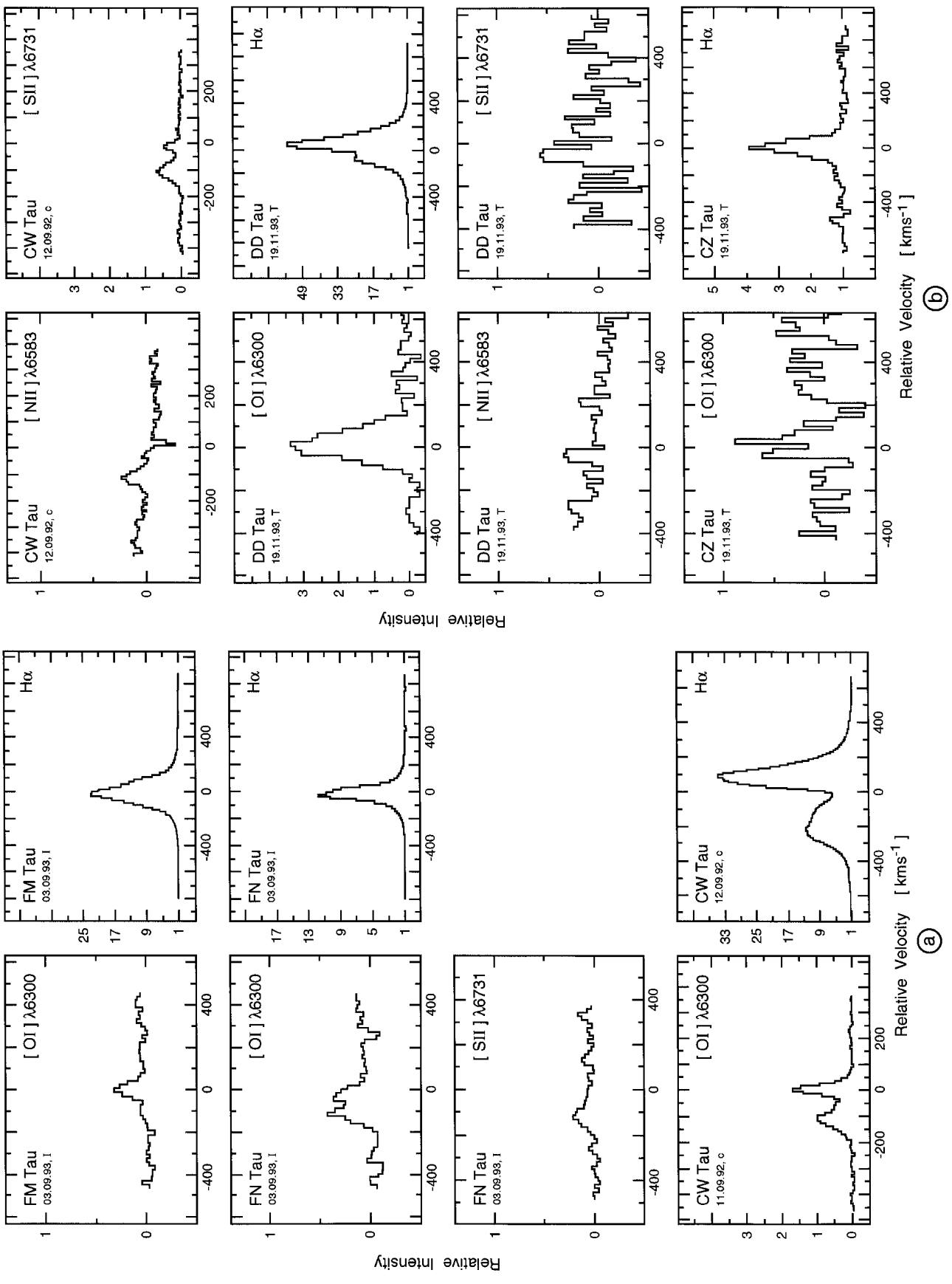
FM Tau
03.09.93, I
[OI] λ6300
Hα
FN Tau
[SII] λ6731
CW Tau
11.09.92, c
12.09.92, c
DD Tau
19.11.93, T
CZ Tau
[NII] λ6583
Relative Intensity
Relative Velocity [kms-1]
a
b

Fig. 22.

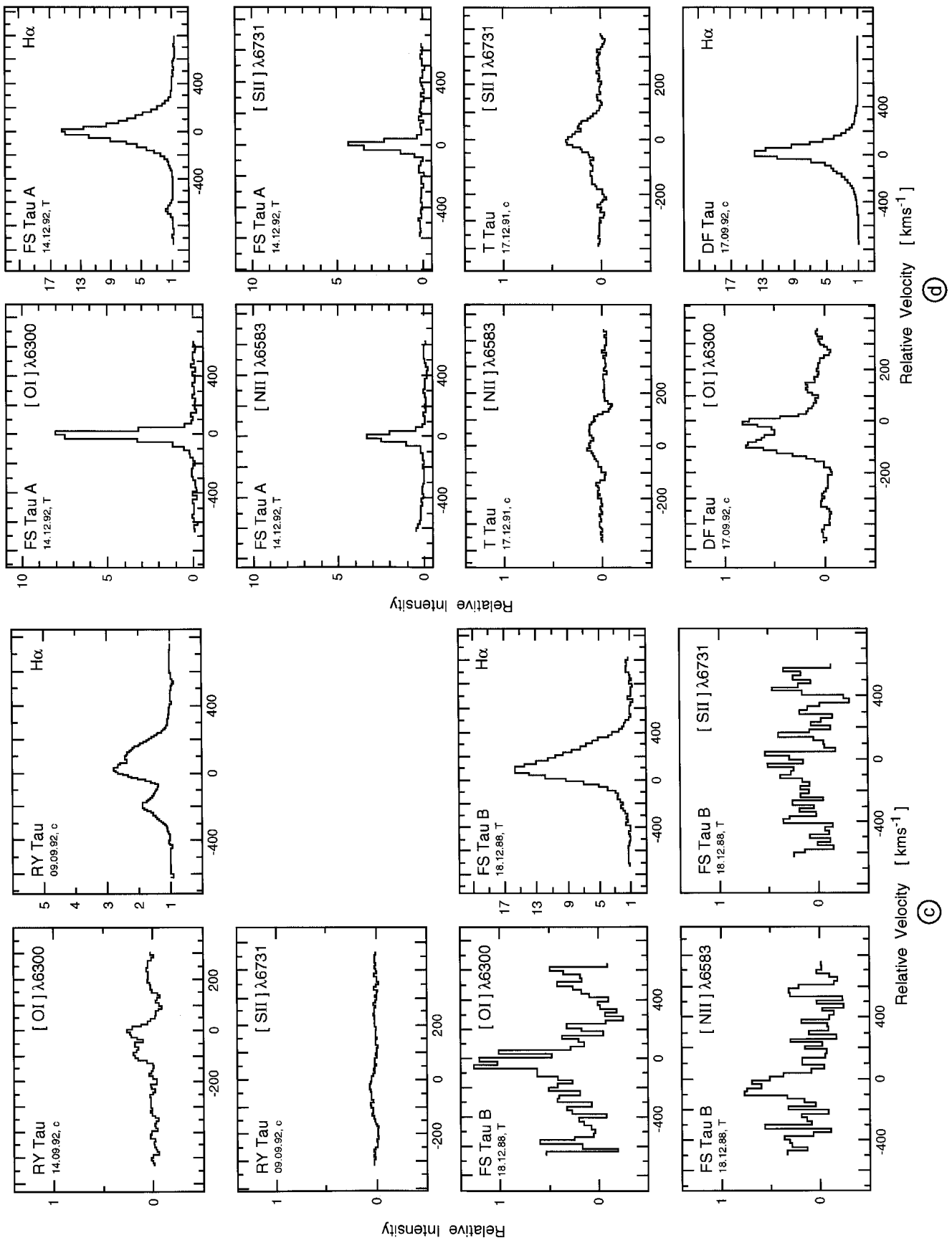

Fig. 22. continued

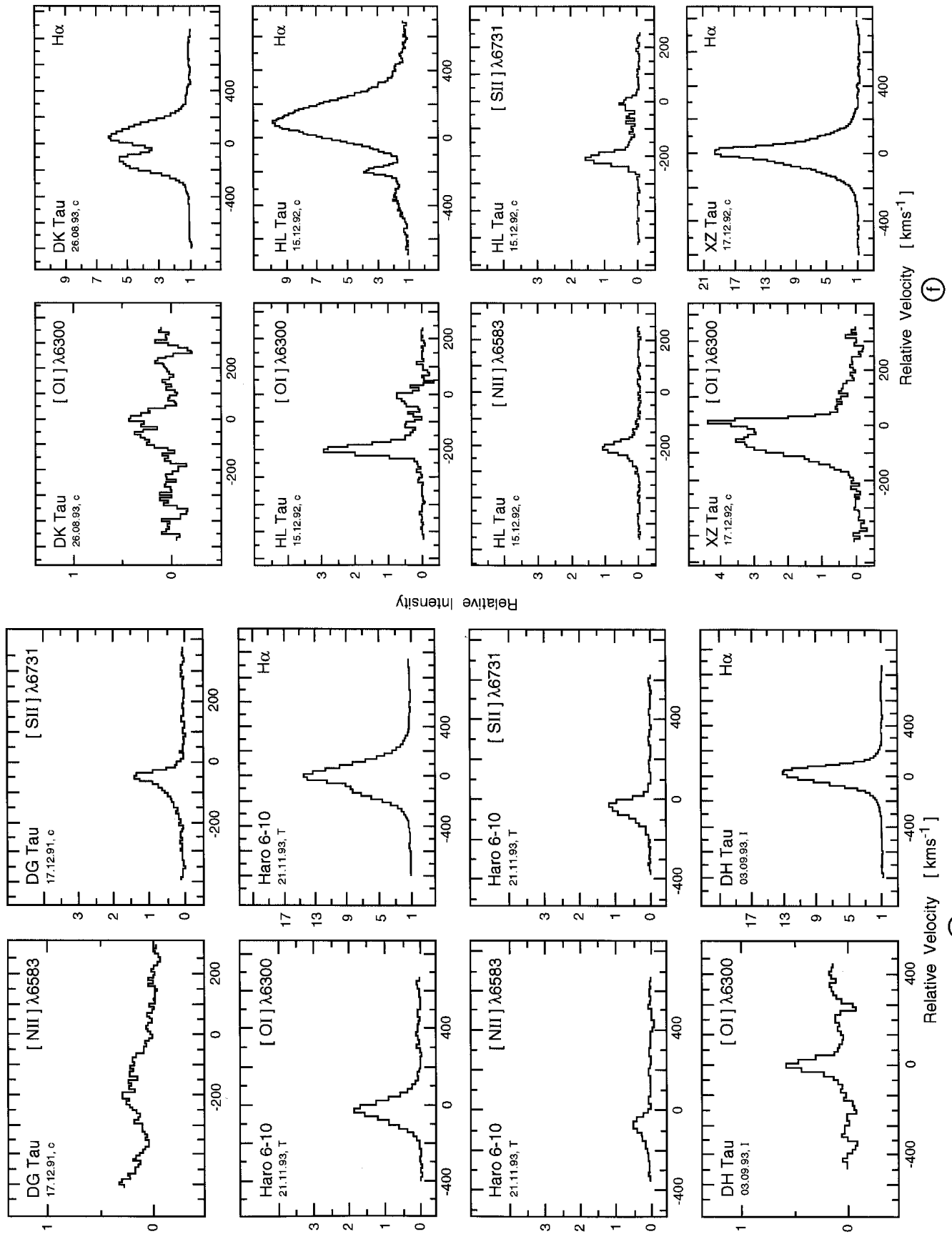

Fig. 22. continued

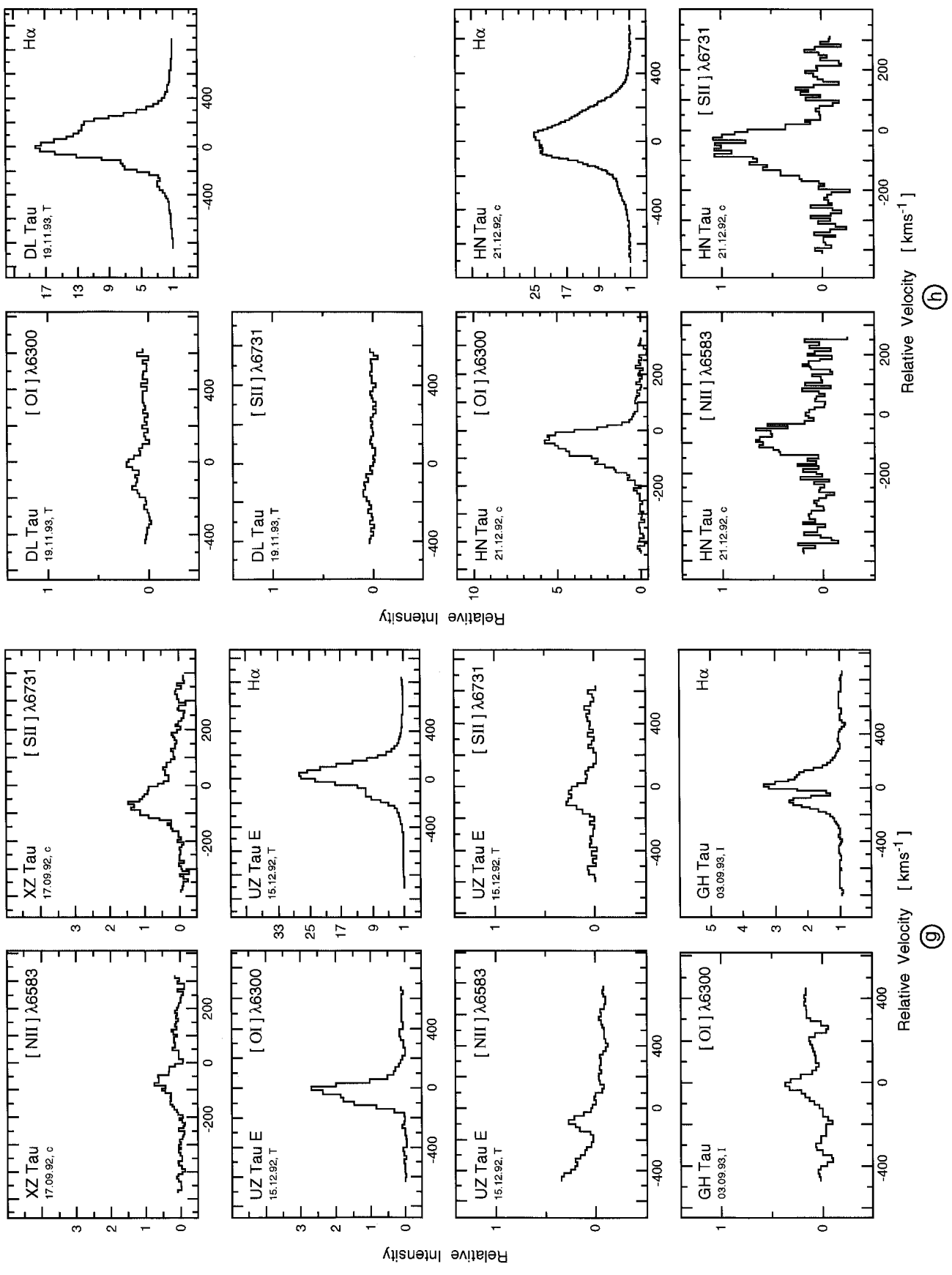

Fig. 22. continued

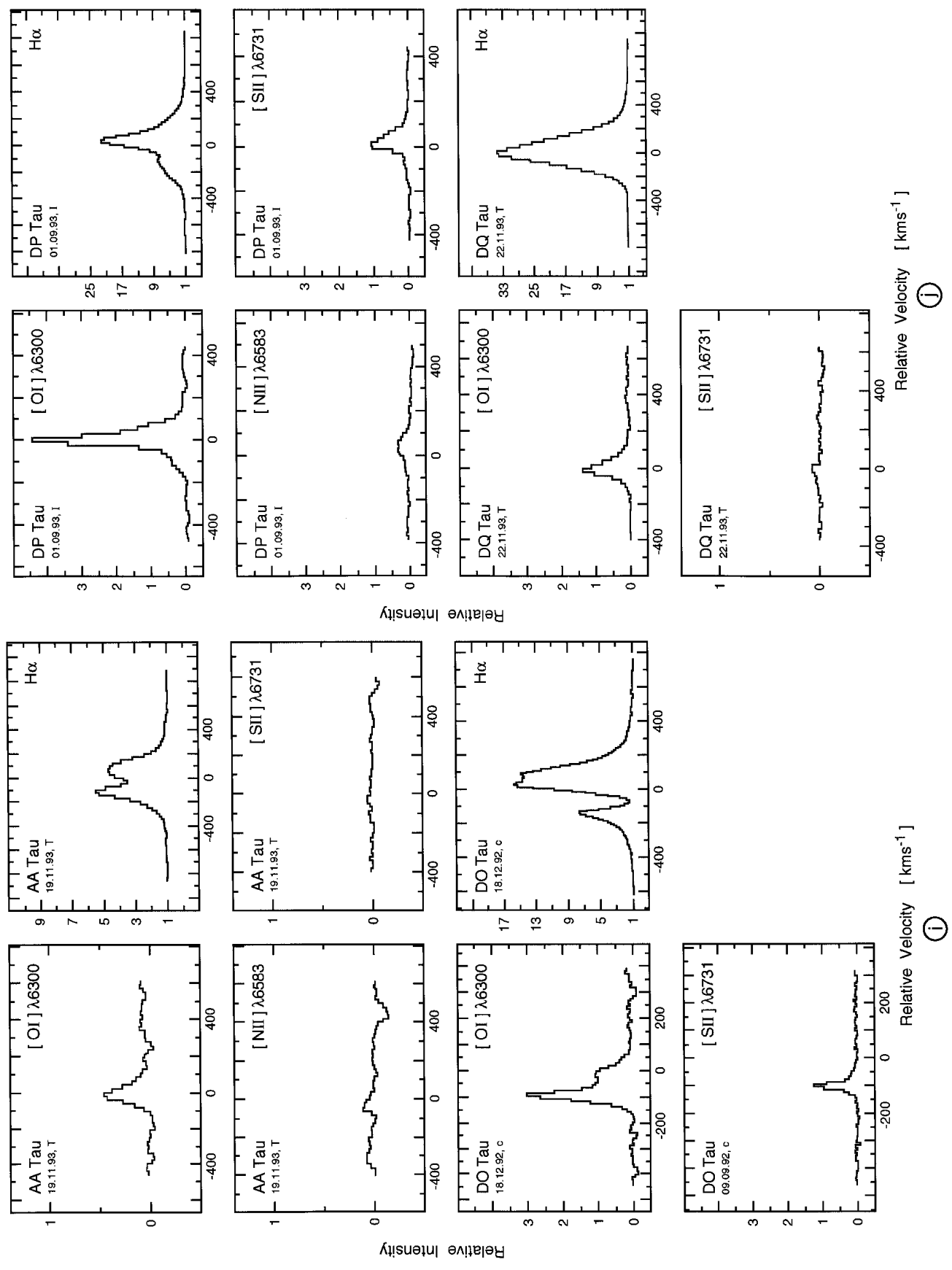

Fig. 22. continued

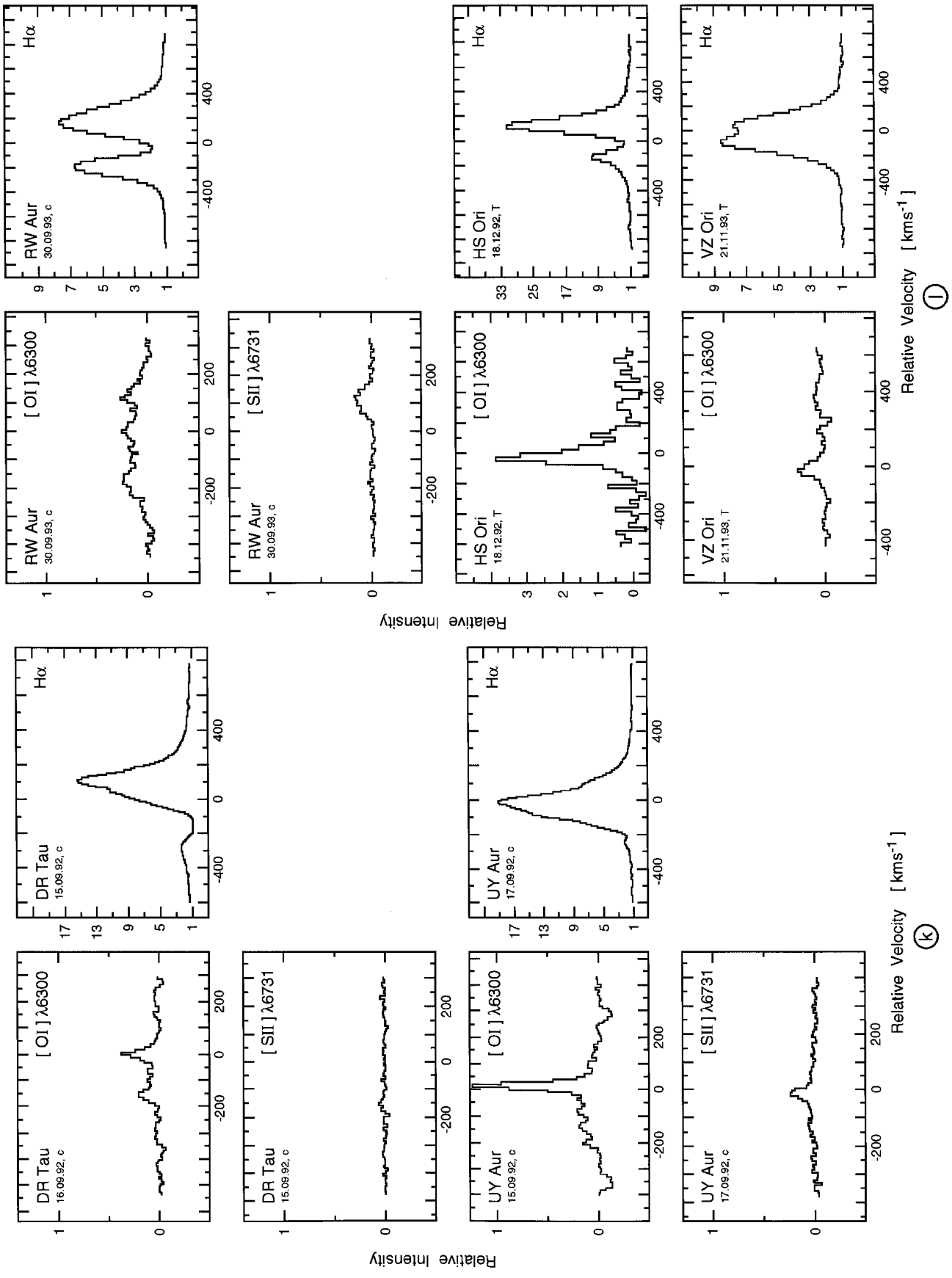

Fig. 22. continued

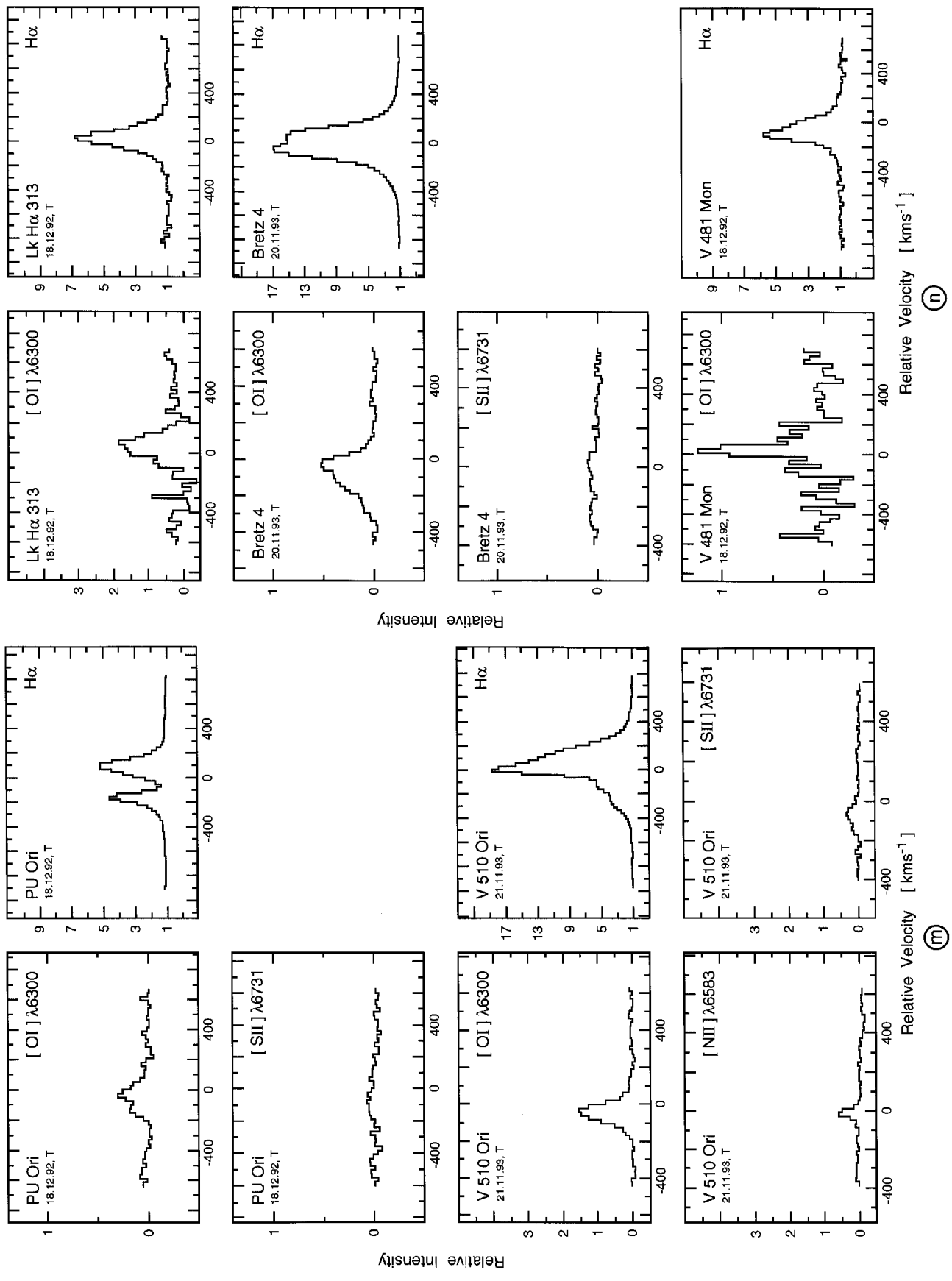

Fig. 22. continued

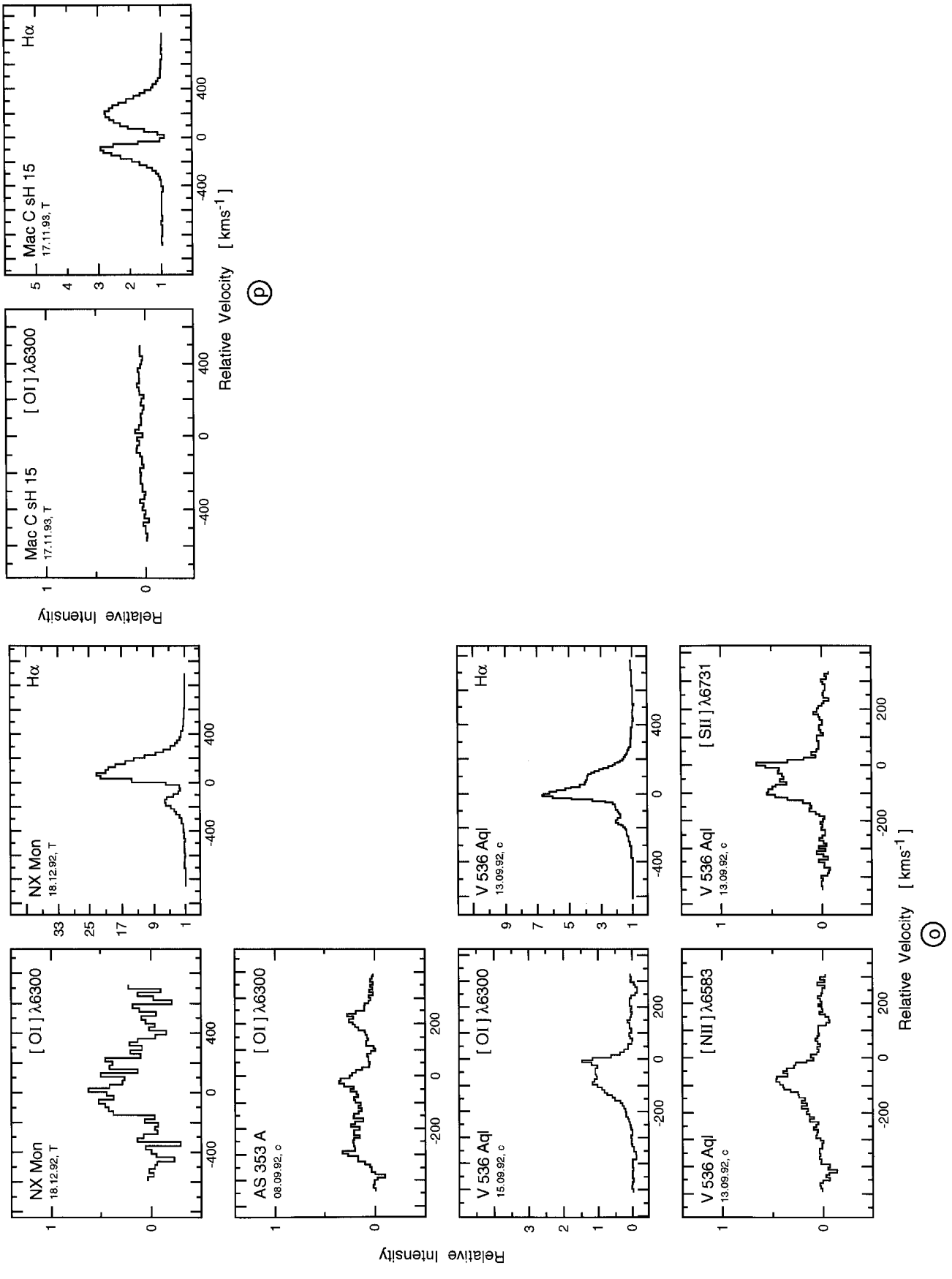

Fig. 22. continued